INTERNATIONAL JOURNAL OF CLIMATOLOGY
Int. J. Climatol. (2018)
Published online in Wiley Online Library
(wileyonlinelibrary.com) DOI: 10.1002/joc.5446

Spatial variations and trends in AOD climatology over East Africa during 2002–2016: a comparative study using three satellite data sets

Richard Boiyo,[a,b] K. Raghavendra Kumar[a]* and Tianliang Zhao[a]*

[a] *Collaborative Innovation Centre on Forecast and Evaluation of Meteorological Disasters, Key Laboratory of Meteorological Disaster, Ministry of Education (KLME), International Joint Laboratory on Climate and Environment Change (ILCEC), Key Laboratory for Aerosol-Cloud-Precipitation of China Meteorological Administration, School of Atmospheric Physics, Nanjing University of Information Science and Technology, Nanjing, China*

[b] *Department of Physical Sciences, Meru University of Science and Technology, Kenya*

ABSTRACT: Aerosol optical depth (AOD) has become one of the most crucial parameters for climate change assessment. This study presents long-term (2002–2016) spatio-temporal distributions and trends in AOD over East Africa (EA) retrieved from the moderate-resolution imaging spectroradiometer (MODIS) Aqua [Dark Target (DT) and Deep Blue (DB)] and multi-angle imaging spectroradiometer (MISR). An inter-comparison of AODs retrieved from different algorithms noticed significant positive correlations ($r = 0.72 - 0.87$) with MISR underestimating MODIS. Moderate (>0.5–0.8) to high (≥0.8) correlations in AOD exhibited over EA, with a few regions representing low (0–0.5) positive correlations. The spatial patterns of annual mean AOD were generally characterized by low (<0.2), moderate (0.2–0.35) and high (>0.35) centres over EA. The seasonal mean AODs over EA were found high (low) during the local dry (wet) seasons, with annual mean ($\pm\sigma$) values of 0.20 ± 0.01, 0.18 ± 0.01 and 0.20 ± 0.02 as observed by DT, DB and MISR, respectively. A single peak distribution of frequencies in AOD was observed by the three sensors in the interval 0.1–0.2, signifying a generally less polluted environment dominated by particular aerosol type. Linear trend analysis revealed an increase in AOD by 0.52, 0.57 and 0.74% year^{-1} as detected by MISR, DT and DB, respectively, and were consistent with those noted in key meteorological parameters. Furthermore, annual and seasonal spatial trends and tendencies revealed a general increase in AOD over EA, being positive and significant over the northern part of EA. Later, classification of major aerosol types over major cities in EA revealed dominance of continental (74.47%) followed by the mixed (16.22%) and biomass-burning/urban-industrial (8.02%) aerosols, with minor contributions from desert dust (1.03%) and clean maritime (0.32%) type of aerosols.

KEY WORDS MODIS; MISR; AOD; spatial trends; aerosol-type classification; East Africa

Received 17 July 2017; Revised 4 January 2018; Accepted 8 January 2018

1. Introduction

Atmospheric aerosols are amongst the major climate forcing agents recognized globally (Charlson *et al.*, 1992; IPCC, 2013). Aerosols influence climate directly by scattering and absorbing solar and terrestrial radiations and indirectly by modifying cloud formation properties (Twomey, 1977; Albrecht, 1989; Haywood and Boucher, 2000; Zhang and Reid, 2010). Absorption of solar radiation by aerosols leads to warming of the troposphere and cooling of the surface, which can alter atmospheric stability, thereby influencing cloud microphysics and their lifetime (Twomey, 1977; Albrecht, 1989; Guleria *et al.*, 2014). On the other hand, backscattering of solar radiation enhances planetary albedo, exerting negative climate forcing (Charlson *et al.*, 1992; Rosenfeld, 2000). Aerosols cause negative climate forcing by indirectly modifying cloud albedo and droplet size distribution, changing the radiative properties and lifetime of clouds (Ramanathan *et al.*, 2001). They also cause positive feedback by absorbing reflected radiation from the Earth's surface and preventing them from escaping to space. Consequently, they indirectly influence the land surface process, global surface temperature, climate and hydrological cycle and ecosystems (Ramanathan *et al.*, 2001; Huang *et al.*, 2006; Lau *et al.*, 2006; Ramanathan and Feng, 2009).

Despite the progress made in understanding and quantifying the climatic effects of aerosols, many uncertainties still exist as compared to those of greenhouse gases (IPCC, 2013). Part of these uncertainties arises because of incomplete knowledge of aerosol's spatio-temporal distributions, trends and their associated properties (Alam *et al.*, 2011; Mehta, 2015). It is, therefore, important that

* Correspondence to: K. R. Kumar or T. Zhao, Collaborative Innovation Centre on Forecast and Evaluation of Meteorological Disasters, Key Laboratory of Meteorological Disaster, Ministry of Education (KLME), International Joint Laboratory on Climate and Environment Change (ILCEC), Key Laboratory for Aerosol-Cloud-Precipitation of China Meteorological Administration, School of Atmospheric Physics, Nanjing University of Information Science and Technology, Nanjing 210044, China. E-mail: kanike.kumar@gmail.com; krkumar@nuist.edu.cn; tlzhao@nuist.edu.cn

we continue to improve characterization of aerosols over different regions of the globe, particularly specific ones such as East Africa (EA) (Boiyo *et al.*, 2017a, 2017b) which experiences inadequate description of atmospheric aerosols. A number of ways, ranging from field measurements (Moorthy *et al.*, 2005; Robles-Gonzalez and de Leeuw, 2008) to ground (Holben *et al.*, 1998) and satellite-based remote sensing (Remer *et al.*, 2005; Torres *et al.*, 2007), have often been used for the past decades to provide continuous data sets of various aerosol parameters.

Although field measurements provide an accurate and detailed description of aerosols, they are usually limited in space. Furthermore, they require extensive manpower for constant monitoring and maintenance (Bennouna *et al.*, 2011; Kumar *et al.*, 2013, 2017) which eventually results in data gaps. A number of ground-based remote sensing networks such as Aerosol Robotic Network (AERONET) (Holben *et al.*, 1998), European Aerosol Research Lidar Network (EARLINET) (Amiridis *et al.*, 2005), Micro-Pulse Lidar Network (MPLNET) (Welton and Campbell, 2002) and China Aerosol Remote Sensing Network (CARSNET) (Che *et al.*, 2009) procure continuous measurements of aerosol properties in various parts of the globe with very high temporal resolution. However, they require expensive and sophisticated instruments and covers relatively small spatial areas. Recent efforts have also focused on numerical modelling and prediction which is intended to resolve various atmospheric processes such as sources, transformation processes, transport and sinks of aerosols and their precursors. This process is usually associated with large degree of uncertainties related to aerosols processes. Furthermore, they require statistically sophisticated approaches combining observations and models so as to reduce uncertainties related to the model initial conditions (Liu *et al.*, 2011).

In regard to above constraints, much attention has been devoted towards monitoring of atmospheric aerosols using a number of space-borne sensors such as advanced very high-resolution radiometer (AVHRR), total ozone mapping spectrometer (TOMS), multi-angle imaging spectroradiometer (MISR), ozone monitoring instrument (OMI) and moderate-resolution imaging spectroradiometer (MODIS) (Ignatov *et al.*, 2004; Torres *et al.*, 2007). Remote sensing of atmospheric aerosols from space-borne sensors provides unprecedented opportunity to achieve long-term continuous global characterization of aerosols (Kumar *et al.*, 2014a, 2015; Adesina *et al.*, 2016; Boiyo *et al.*, 2017a). However, retrievals from these sensors usually suffer from uncertainties associated with instrument calibration, data coverage, retrieval algorithms, cloud screening and surface properties resulting in different aerosol optical depth (AOD) values for a given space and time (Bennouna *et al.*, 2011; Mehta *et al.*, 2016). In consequence, their reliability in representing spatio-temporal variability and trends in AOD alongside associated properties is an important aspect that needs urgent intervention, especially over the less explored regions such as EA.

One step of ensuring the reliability of satellite-derived AOD products is by carrying out comparative climatologies from more than one sensor. Retrievals from multiple sensors are considered reliable if all the sensors retrieve aerosol parameters with more or less the same strength (Alpert *et al.*, 2012). Several studies focusing on comparative climatologies have been reported in different parts of the globe. Studies by Guleria *et al.* (2012a, 2012b) and Gautam *et al.* (2013) showed the capability of satellites in characterizing AOD distribution over locations having a typical topography. Mehta (2015) reported comparable spatial variations in AODs retrieved by the MODIS and MISR sensors. A significant positive correlation in AODs retrieved by the MODIS and MISR was reported by Kumar *et al.* (2015) over Durban, South Africa (SA), while Adesina *et al.* (2016) reported declining AOD trends retrieved from the sensors over different regions of SA. Also, Mehta *et al.* (2016) reported a good agreement in AOD variations and trends retrieved from MODIS and MISR sensors. Furthermore, Kang *et al.* (2016) investigated the spatial-temporal evolution and trends in aerosol optical properties over Yangtze River Delta (China) using MODIS and MISR data. The AODs retrieved from MISR sensor were consistently lower than those derived from MODIS. Recently, a consistent spatial variation in aerosol optical properties and identification of aerosol types from different clustering techniques were reported by Kumar *et al.* (2018) over an urban-industrially polluted city, Nanjing in east China.

EA is one of the regions around the globe that deserves better and extensive characterization of aerosols in terms of spatio-temporal distribution, trends and associated properties. It is currently experiencing an unprecedented increase in aerosol concentration due to growing population, rapid urbanization and industrialization, climate change and lack of strict environmental policies geared towards minimizing emissions (Van Vliet and Kinney, 2007; Ngo *et al.*, 2015; Egondi *et al.*, 2016). The proximity of region to the Indian Ocean, Sahara Desert and central Africa's Democratic Republic of Congo (DRC) makes it vulnerable to almost all types of aerosols (Makokha and Angeyo, 2013; Boiyo *et al.*, 2017a). Despite this, it continues to lag behind the rest of the world in studies related to atmospheric aerosols, with far-reaching consequences on its inability to quantify precisely the climatic impacts of atmospheric aerosols. Previous studies over the region (Makokha and Angeyo, 2013; Ngaina and Muthama, 2014) were limited either in terms of area coverage, data span period or analysis techniques and therefore unable to establish comparative AOD climatology. Recent studies (Boiyo *et al.*, 2017a) focused on analysing the spatio-temporal characteristics of aerosol optical properties derived from the MODIS and OMI sensors. In their latest work (Boiyo *et al.*, 2017b), they validated AODs retrieved from MODIS-Terra (DT and DB), MISR and OMI sensors against the ground-based AERONET measurements over selected stations in Kenya, EA. However, the consistencies of the satellite-derived AOD in representing the spatial and temporal variabilities and trends in AOD alongside associated properties over the same region were not examined.

As a continuation of our previous works over EA, the present study seeks to compare the spatio-temporal variability and trends in AOD patterns retrieved from two space-borne sensors: MODIS Aqua (DT and DB) and MISR during 2002–2016, with intent of identifying the similarities and differences between the data sets in characterizing AOD climatology. To achieve this, an inter-comparison and correlation of AOD data sets retrieved from the sensors are first analysed in order to understand their sensing capabilities. The study then synthesizes and compares the spatio-temporal distributions of AOD retrieved from the three sensors. This is followed by a comprehensive analysis of trends and relative changes (tendencies) in AOD, and their potential association with trends in key meteorological factors. In addition, the annual frequency distribution curves of AODs retrieved from the sensors are constructed, followed by an investigation of the dominant aerosol types over three major cities representative of EA. The rest of this article is structured as follows: Section 2 illustrates the study area, data and methodology, while Section 3 details results and discussion. Conclusions and recommendations drawn from the present study are elucidated in Section 4.

2. Materials and methods

2.1. Study region and meteorology

The study domain covers three countries in EA (Kenya, Uganda and Tanzania) enclosed within latitudes 12°S–5°N and longitudes 28°–42°E. It is bordered by Ethiopia and Sudan to the north, Somalia and the Indian Ocean to the east, Rwanda, Burundi and DRC to the west and Mozambique and Zambia to the south (Boiyo *et al.*, 2017a). The region experiences tropical climate with climatic variations influenced by several factors such as Inter-Tropical Convergence Zone (ITCZ), El Nino-Southern Oscillation (ENSO) and Indian Ocean Dipole (IOD) (Ongoma and Chen, 2017). Based on the prevailing meteorological conditions, a year has been divided into four seasons: March–May (MAM), June–August (JJA), September–November (SON) and December–February (DJF) for further analysis in this study. Higher amounts of precipitation are generally observed from March to May (MAM, 'long rains') and September to November (SON, 'short rains') resulting in large wet deposition (rainout) of aerosols (Figure 1(a)). In contrast, the local dry seasons (June–August; JJA and December–February; DJF) are characterized by high aerosol loadings associated with reduced precipitation (Figure 1(a)) (Makokha and Angeyo, 2013; Ngaina and Muthama, 2014).

Apart from the aerosol data, this study investigated prevailing climatic condition and trends in temperature (°C), wind speed ($m\,s^{-1}$), relative humidity (%) and total precipitation (mm). The monthly averaged temperature, wind speed and relative humidity at 850 hPa and spatial resolution of $0.75 \times 0.75°$ were sourced from the European Centre for Medium-Range Weather Forecasts (ECMWF), previously used by a number of authors over EA (Yang *et al.*, 2015; Ogwang *et al.*, 2016). However, the Climate Research Unit (CRU) temperature (Harris *et al.*, 2014) and Tropical Rainfall Measuring Mission (TRMM) (Huffman *et al.*, 2007) precipitation data sets derived at spatial resolutions of $0.5 \times 0.5°$ and $0.25 \times 0.25°$, respectively, were preferred due to their better performance over the region (Kerandi *et al.*, 2017; Makokha *et al.*, 2017).

Temperatures over EA were found to be moderate in the range 14–30 °C (Figure 1(b)), with the lowest (highest) values generally observed during JJA (DJF). Relative humidity (in the range of 40–85%) showed significant seasonal heterogeneity being high during MAM and low during DJF (Figure 1(c)). The study region is drier during JJA followed by SON, being more intense in the southwest part of Tanzania during these seasons. The synoptic winds patterns are predominantly easterlies with significant seasonality in direction and magnitude (Figure 1(d)). The DJF is dominated by north easterlies carrying significant amount of dust from the Arabian and Saharan Deserts at certain times of the year (Boiyo *et al.*, 2017a). MAM and JJA are dominated by south easterlies which enhances production and transportation of marine aerosols and smoke particles from the southwest Indian Ocean and Madagascar Island, respectively. It has also been established that during JJA, winds at 850 hPa are characterized by westerly flow between 25°–30°E and 5°–10°N associated with air masses transported from the DRC (Ogwang *et al.*, 2016). These air masses could transport significant amount of smoke particles to the study domain (Boiyo *et al.*, 2017a).

2.2. Instrumentation and data

2.2.1. The MODIS sensor

The MODIS sensor was launched into the Earth's orbit with daytime equator crossing at 1030 LST (UTC + 3) by the National Aeronautics and Space Administration (NASA) Goddard Space Flight Center (GSFC) on 18 December 1999 onboard the Terra satellite. The second was launched on 4 May 2002 onboard the Aqua platform (Remer *et al.*, 2005) and has daytime equator crossing at 1330 LST. The sensor has a swath of ∼2330 km, with a temporal resolution of 1–2 days and acquires data over 36 spectral bands ranging in wavelengths from 0.415 to 14.235 μm at three spatial resolutions (2 bands at 250 m, 5 bands at 500 m and 29 bands at 1 km) (Mito *et al.*, 2012; Hu *et al.*, 2017). Seven of these bands operating in near-ultraviolet (UV), visible and near-infrared spectroscopy (IR) wavelength regions (0.415–2.155 μm) can effectively retrieve AOD over land and ocean (Hsu *et al.*, 2013; Sayer *et al.*, 2013, 2014) using two different algorithms: 'Dark Target (DT)' and 'Deep Blue (DB)'. The two algorithms are based on Look Up Table (LUT) approach that employs pre-defined set of aerosol types, loadings and geometries (Floutsi *et al.*, 2016).

The difference between DT and DB arise in the manner, in which they account for the removal of the surface reflectance signal to accurately determine the aerosol signal (Mehta *et al.*, 2016). DT employs a set of ratios

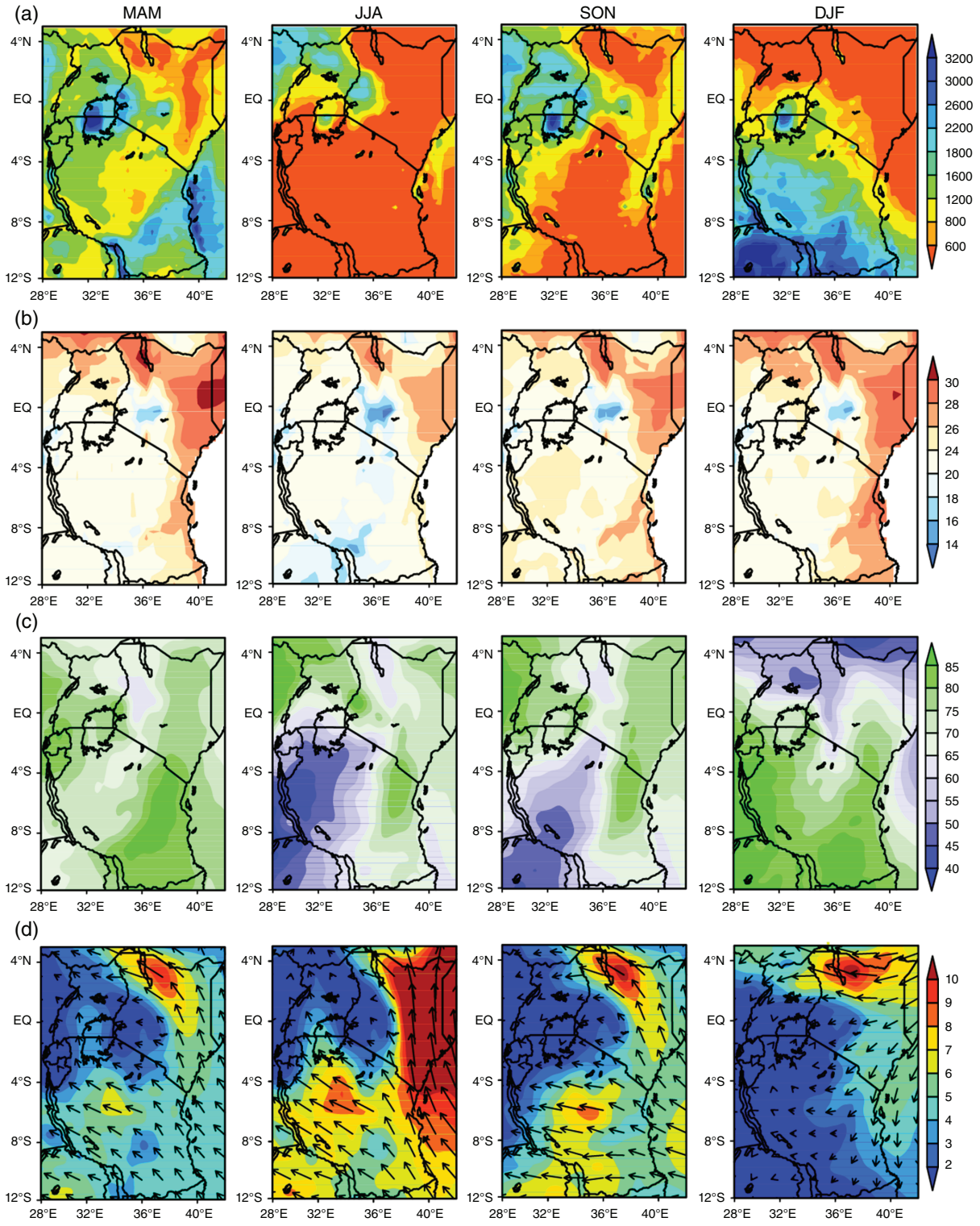

Figure 1. The seasonal variations of (a) accumulated precipitation (in mm), (b) temperature (in °C), (c) relative humidity (in %) and (d) wind speed (in $m\,s^{-1}$ indicated by colour shades) and wind direction (in degrees shown by arrows) derived from the ECMWF during 2002–2016 over the study domain. [Colour figure can be viewed at wileyonlinelibrary.com].

and relationships between 0.47, 0.67 and 2.1 μm channels to account for the surface signal and works best over dense, dark vegetated targets as compared to bright land surfaces. DB uses maps and libraries of surface reflectance in the blue channels to account for the surface signal as well as spectral reflectance ratios. It was originally developed to fill gaps in DT by providing coverage over brighter land surfaces such as desert areas; but later improved to retrieve aerosols over most vegetated targets and all cloud-free, snow-free land surfaces resulting in 'enhanced Deep Blue' algorithm (Hsu *et al.*, 2004, 2006, 2013).

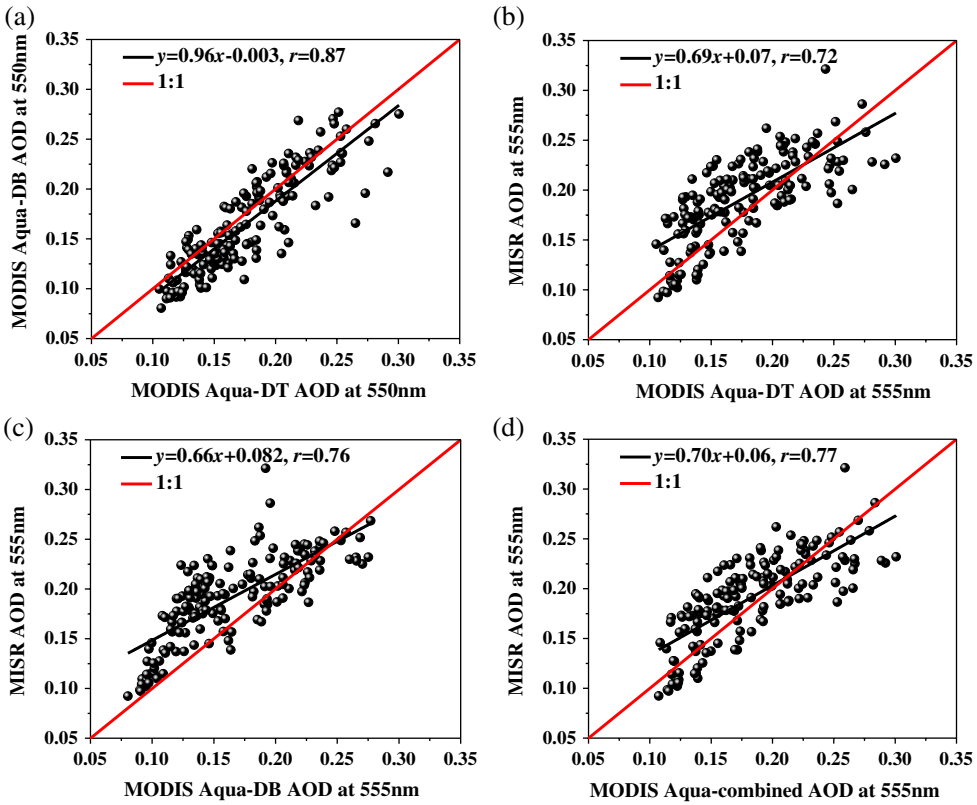

Figure 2. Inter-comparison of AODs retrieved from (a) MODIS Aqua-DB *versus* MODIS Aqua-DT, (b) MISR *versus* MODIS Aqua-DT, (c) MISR *versus* MODIS Aqua-DB and (d) MISR *versus* MODIS Aqua-combined over EA during 2002–2016. The red and black solid lines in all panels represent 1:1 and linear regression fittings, respectively. The corresponding regression coefficients obtained from the fitting are also shown in all panels, with '*r*' being the correlation coefficient. [Colour figure can be viewed at wileyonlinelibrary.com].

MODIS aerosol products are stored at different levels and under various versions called 'Collections'. The MODIS data processing levels include Level 1.0 (geolocated radiance and brightness temperature), Level 2.0 (retrieved geophysical data products) and Level 3.0 (gridded points). The MODIS aerosols retrieval is calculated on a 10×10 km resolution (Level 2), which is retrieved from higher-resolution radiance measurements (Level 1B). Clouds are screened within the Level 2 box (Levy *et al.*, 2007) and the aerosol retrievals are performed if there is sufficient number (approximately 10%) of non-cloudy pixels. Hence, Level 2 products may be valid even when the box has cloud coverage of ~90%. Depending on the quality of the retrieval (and the number of valid pixels), the 10-km retrieval is assigned a quality assurance (QA) value. The 10-km retrievals are aggregated to the 1° box (Level 3). MODIS retrieval accuracy over land and Ocean (Tanré *et al.*, 1997; Remer *et al.*, 2005) were estimated to be $\pm 0.05 \pm 0.20$ (AOD) and $\pm 0.03 \pm 0.15$ (AOD), respectively, for Level 2 products. This work utilized Collection 6 (C006) Level 3 daily and monthly AOD_{550} retrieved from the MODIS Aqua (DT and DB) at a spatial resolution of $1 \times 1°$ for a period of 14 years (June 2002–May 2016). In addition, daily averaged Ångström exponent in the spectral range 470–660 nm ($AE_{470-660}$) derived from the MODIS Aqua-DT were used to investigate the dominant aerosol types over three major cities (Nairobi, Kampala and Dodoma) representative of EA. The MODIS Aqua aerosol data products were preferred in this study due to greater availability of valid pixels over EA and relatively high (1–2 days) temporal resolution (Levy *et al.*, 2010). These data products were sourced from the NASA LAADS (http://ladsweb.nascom.nasa.gov/). Detailed information about the sensor, data products, retrieval algorithms, calibration and uncertainties can be found elsewhere (Hsu *et al.*, 2004, 2006, 2013; Levy *et al.*, 2007; Sayer *et al.*, 2013, 2014, 2015).

2.2.2. *The MISR sensor*

The MISR is a passive radiometer also launched onboard the Terra platform in 1999 by NASA. It observes reflected and scattered sunlight in four spectral bands (centred at 446, 558, 672 and 866 nm) in nine different directions (four forwards, four backwards and nadir) both over land (desert included) and ocean (Diner *et al.*, 2001; Kahn *et al.*, 2010). This unique design enables it to retrieve AOD over high reflecting surfaces such as arid and semi-arid areas in the north of EA. The global coverage time is every 9 days with repeat coverage between 2 and 9 days depending on the latitude. The AOD retrieval algorithm is also based on LUT approach, but the algorithm is dependent on surface types such as densely vegetated areas, dark water bodies or high contrast terrain (Diner *et al.*, 2001). Validation results with the AERONET (Diner *et al.*, 2001; Kahn

et al., 2010) have shown the retrieval accuracy of ±0.05 or ±0.20 (AOD), whichever is higher. This work utilized the MISR Terra Level 3 monthly averaged AOD_{555} at a spatial resolution of $0.5 \times 0.5^{\circ}$ obtained from Giovanni online analysis and visualization system (GIOVANNI) (http://giovanni.gsfc.nasa.gov/giovanni/) during the same duration as MODIS Aqua AOD. The MISR data were used for the inter-comparison with reliability achieved when two or more algorithms show more or less similar results (Alpert *et al.*, 2012; Adesina *et al.*, 2016).

2.3. Methodology

An inter-comparison of satellite-derived AOD from different algorithms is required in order to understand the sensing capabilities of the instruments, achieve long-term AOD database for climatological studies, as well as improve the accuracy and coverage achievable with a single sensor (Alam *et al.*, 2011; Kumar *et al.*, 2015). For this purpose, MODIS Aqua AOD was first interpolated logarithmically to MISR-derived AOD using the Ångström power law (Ångström, 1961), previously used by a number of authors (Tripathi *et al.*, 2005; Prasad and Singh, 2007; Kumar *et al.*, 2014a) over different environments. In order to compute correlations and differences in satellite-derived AODs, the original MISR-derived AOD at a spatial resolution of $0.5 \times 0.5^{\circ}$ was rescaled to $1 \times 1^{\circ}$ resolution in order to be consistent with the MODIS-based AOD. The rescaling was performed by assigning equal weights to each sub-grid, and the final $1 \times 1^{\circ}$ considered valid only when more than half of the sub-grids have valid data.

The relative change in AOD (which relates the current with initial AOD values) can be used to quantitatively describe the inter-annual variations in AOD. In the present work, the annual and seasonal relative changes in AOD (in decimal form) are computed using the expression:

$$\text{Relative AOD change}_{a(s)} = \frac{\text{Average AOD } (2009-2016)_{a(s)} - \text{Average AOD } (2002-2008)_{a(s)}}{\text{Average AOD } (2002-2008)_{a(s)}} \quad (1)$$

where subscripts '*a*' and '*s*' denote annual and seasonal AOD values, respectively.

Several statistical approaches exist to quantify trends in a time series data of a particular geophysical variable. In the present study, linear regression analysis was used to estimate annual and seasonal trends in AOD alongside trends in key meteorological parameters. The method (Weatherhead *et al.*, 1998) previously used in other related studies (Kumar *et al.*, 2014a, 2015; Dahutia *et al.*, 2017) has a practical advantage of simply assessing the direction and magnitude of trend in a long-term data. Following this method, a linear trend model (Equation (2)) was adopted:

$$Y_t = c + \omega * X_t + \varepsilon \quad (2)$$

where Y_t is the geophysical variable for which the trend is being determined, c is the offset (y-intercept) which represents the value of Y_t at the beginning of the time series. X_t is the independent variable representing time, ω is the trend estimate of the geophysical variable under consideration, while ε is the noise in the time series. The statistical significance of the estimated trends was further tested using the method developed by Weatherhead *et al.* (1998). In this regard, trends are considered significant at a p-value of 0.05 or a 95% confidence interval when $\left|\frac{\omega}{\delta}\right| > 2$, whereas trends are considered significant at a 90% confidence level when $1.5 < \left|\frac{\omega}{\delta}\right| < 2$, where δ is the standard deviation of the slope obtained from the linear regression. This method has a practical advantage of assessing the direction and magnitude of variations in a long-term data (Zhang and Reid, 2010; Kumar *et al.*, 2014a, 2015; Dahutia *et al.*, 2017; Hu *et al.*, 2017) and was therefore considered suitable for executing pixel-wise analysis.

A preliminary investigation of major aerosol types found over three representative major cities (Nairobi, Kampala and Dodoma) in EA is carried out via the AOD_{550} *versus* $AE_{470-660}$ relationship, previously used by a number of authors (Kaskaoutis *et al.*, 2007, 2009; Kumar *et al.*, 2014b, 2018; Bibi *et al.*, 2016; Yu *et al.*, 2016) over different environments. As both are spectrally dependent parameters, $AE_{470-660}$ represents the aerosol particle-size, while AOD_{550} is dependent on the aerosol column density. Therefore, AOD_{550} *versus* $AE_{470-660}$ plot qualitatively indicates the amount and dimension of aerosols observed. Different aerosol types were discriminated through determination of physically interpretable cluster regions separated by solid lines that act as threshold values of AOD_{550} and $AE_{470-660}$. The selection of the threshold values is very important and varies depending on the geographical locations. In the present study, the AOD_{550}, $AE_{470-660}$ pair ranged between (0.015–1.63, 0.1–1.8), (0.012–0.949, 1.037–1.8) and (0.015–1.28, 0.206–1.8) over Nairobi, Kampala and Dodoma, respectively. Therefore, the threshold values for constructing the scatter diagram are slightly changed from those previously used by a number of authors (Kaskaoutis *et al.*, 2007; Kumar *et al.*, 2018). Therefore, $AOD_{500} < 0.2$ with large (>1) or small (<0.9) values of $AE_{470-660}$ corresponded to continental clean (CCB) aerosols representing background conditions over the three locations and clean maritime-influenced aerosols (CMA), respectively. However, $AOD > 0.3$ and $AE > 1.0$ corresponds to turbid atmospheric condition dominated by biomass-burning aerosols and/or urban/industrial plumes (BUI), while very high turbid atmospheres with $AOD_{550} > 0.6$ and $AE_{470-660} < 0.7$ is used to indicate dust aerosol type (DDT) (Adesina *et al.*, 2017). The remaining gaps, considered as mixed-type aerosols (MXD), reveal cases where aerosols are difficult to be discriminated bearing in mind effects of various aerosol-mixing processes in the atmosphere such as coagulation, condensation, humidification and gas-to-particle conversion (Pace *et al.*, 2006).

3. Results and discussion

3.1. Inter-comparison and spatial correlations of AOD data sets

The paired monthly averaged MODIS Aqua (DT and DB) and MISR fitted with 1:1 and regression fitting lines, and the corresponding statistical parameters obtained over EA are shown in Figure 2. The DB *versus* DT AOD correlation was found to be strongest ($r = 0.87$) followed by MISR *versus* DB ($r = 0.76$), and MISR *versus* DT ($r = 0.72$). The latter two correlations were less strong due to differences in instrument characteristics and the retrieval algorithms (Tripathi *et al.*, 2005; Kumar *et al.*, 2015). During the study period, MISR systematically underestimated AOD (slopes <1) with respect to DT and DB by 31 and 34%, respectively, while DB slightly underestimated DT by 4%. As expected, the 'merged product' (combining MODIS Aqua DT and DB AOD products) showed a relatively higher correlation with MISR ($r = 0.77$) than either of the original AOD product. This is because the product utilizes the strength of each of the retrieval algorithm significantly reducing the fraction of pixels with no data, thus increasing the spatial coverage of a multitude of surface types ranging from oceans to bright deserts. It should, however, be noted that the performance of each of the algorithm is likely to change depending on dominating aerosol type, underlying surface characteristics, pollution levels and seasonality in emission sources (Tripathi *et al.*, 2005; Kahn *et al.*, 2010).

In order to get deeper insights into the performance of the algorithms, revealing areas of similarities/dissimilarities and their magnitudes, the correlations and differences in AODs were computed for each pixel on annual basis (Figure 3). The moderate (>0.5–0.8) to high (≥0.8) DT–DB correlations over most areas of the study domain indicates that the two algorithms recorded a more or less similar AODs owing to the same sensor platforms. However, the low (0–0.5) DT–DB correlation over the arid and semi-arid areas of northwest of Kenya correspond to zones where DT overestimated DB (Figure 3(d)). On the other hand, moderate to high DT/DB–MISR correlations (Figures 2(b) and (c)) dominated zones with low surface reflectivity such as southwest borders of Uganda and Tanzania with high vegetation cover. However, low DT/MISR correlation characterized the high reflecting arid and semi-arid areas of northern Kenya and Tanzania where DT underestimated MISR (Figure 3(e)). In most cases, AODs retrieved by the MISR and MODIS Aqua DB (Figure 3(f)) showed highest correspondence in terms of area coverage with moderate to high correlation. However, low correlations amongst the algorithms over western parts of Kenya correspond to zones with missing AOD (Figures 4(b) and (c)). This is due to frequent cloud cover leading to insufficient DT/DB and MISR data points, hence weaker data analysis. Also, the differences in the sensors overpass time and retrieval algorithms could interpret the low DT/DB–MISR correlations in some areas of EA (Boiyo *et al.*, 2017b). Despite these, the AODs retrieved by the three algorithms were similar in most areas of the study domain, with the differences amongst the data sets being generally less than ±0.05 (Figures 3(d)–(f)).

3.2. Spatial distributions

3.2.1. Annual distributions of AOD

AOD constitute an important parameter of atmospheric aerosols and could be used to quantify columnar aerosol burden in the atmosphere (Luo *et al.*, 2014; Kumar *et al.*, 2015). The climatological patterns of annual mean AOD derived from MODIS Aqua (DT and DB) and MISR over EA during the study period are shown in Figures 4(a)–(c), respectively. The spatial patterns of annual mean aerosol loading were generally characterized by low, moderate and high AOD indicating distinct features of aerosol load. Low (<0.2) AOD centres were observed by the sensors over highly vegetated areas, with relatively high altitude (Boiyo *et al.*, 2017a) and precipitation (Figure 1(a)) over western and central parts of Kenya, and central and south-eastern parts of Tanzania. Connecting the low AOD centres, DT and DB isolated the volcanic centre along the Kenya–Tanzania border with moderate (0.2–0.35) AOD values. Moderate to high (>0.35) AOD values were also observed by the sensors over arid and semi-arid areas of eastern and northern parts of Kenya with high temperatures (Figure 1(b)). This could be attributed to long-range transport of dust aerosols by the north easterlies (Figure 1(d)) together with those locally produced (Gatebe *et al.*, 2001; Ngaina and Muthama, 2014). Also, the carbonaceous aerosols from the alkaline Lake Turkana resulted in advection of aerosols to high AOD (Boiyo *et al.*, 2017a). A slight difference was, however, observed in the magnitude of AOD values retrieved by the sensors along the borders of southwest of Uganda (over DRC) with high vegetation cover. DT, by virtue of its effective retrieval algorithm over dark surfaces, showed moderate to high AOD values, while the DB and MISR recorded moderate AOD values, all associated with long-range transport of smoke particles from the DRC (Gatebe *et al.*, 2001; Boiyo *et al.*, 2017a). The moderate to high AOD values along the borders of southwest of Uganda could also be associated with strong anthropogenic activities (e.g. biomass burning and forest fires) dominant in the region which contribute significant amount of fine-mode particles into the atmosphere. Also, the stronger westerlies (Figure 1(d)) could transport smoke particles from DRC to this area, increasing the aerosol load. Additionally, the EA's population, topography, aerosol–climate interactions and economy play an important role in influencing aerosol distribution over the study domain.

3.2.2. Seasonal distribution of AOD

The seasonal patterns of AOD over EA derived from MODIS Aqua (DT, DB) and MISR (Figures 5(a)–(c)) are consistent with the respective annual patterns (Figures 4(a)–(c)). In terms of area coverage and strength, the regional aerosol load was found to be high during JJA followed by DJF and SON, and minimum during MAM.

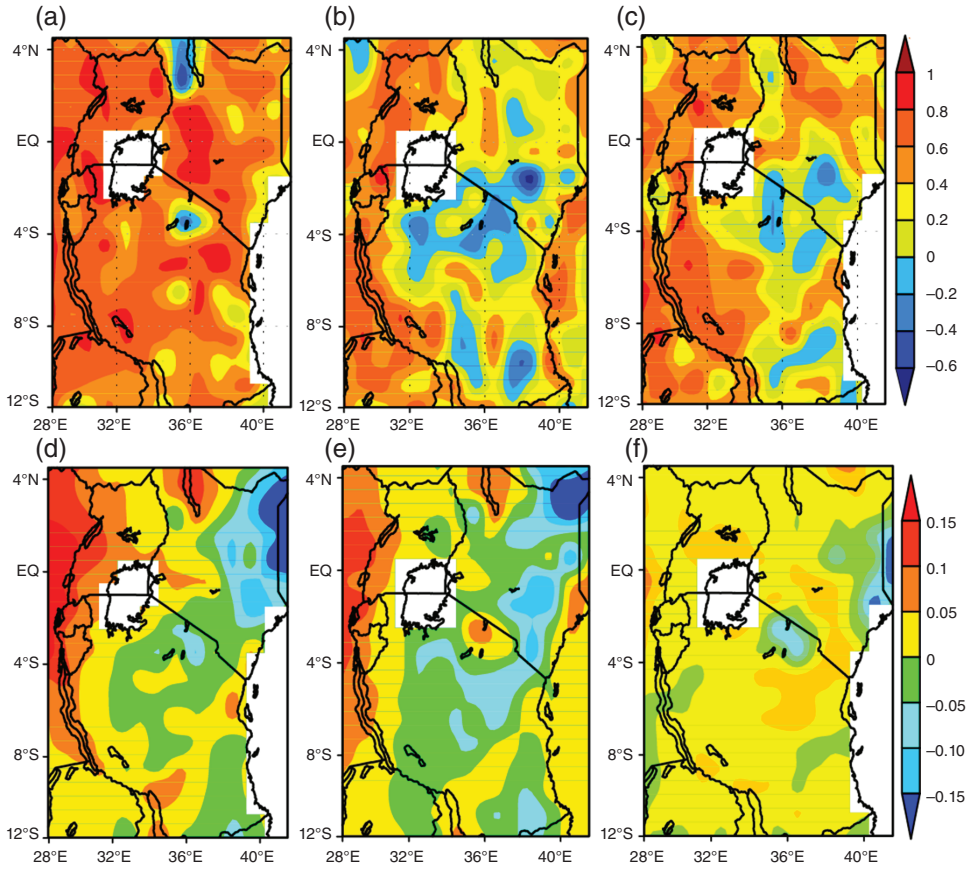

Figure 3. Spatial correlations and AOD differences, respectively, between MODIS Aqua-DT and -DB (a, d), MODIS Aqua-DT and MISR (b, e) and MODIS Aqua-DB and MISR (c, f) over EA during 2002–2016. The colour scale represents the magnitude of correlation coefficient and AOD differences. [Colour figure can be viewed at wileyonlinelibrary.com].

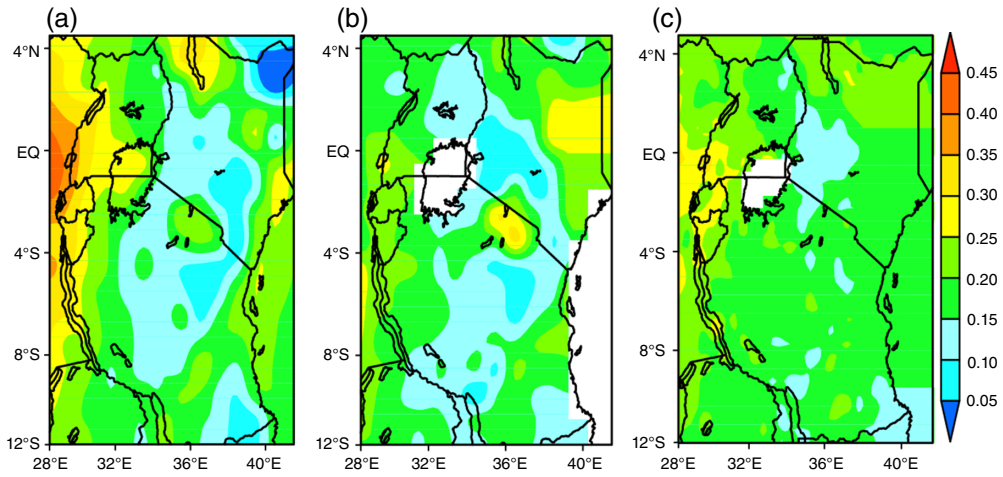

Figure 4. Spatial distribution of annual mean AOD derived from (a) MODIS Aqua-DT, (b) MODIS Aqua-DB and (c) MISR over EA during 2002–2016. [Colour figure can be viewed at wileyonlinelibrary.com].

The seasonality in AOD over EA is more pronounced in high AOD centres depending on the seasonal variations of aerosol sources. During the local dry seasons, high AOD values were noticed over the dust dominant zones of northwest and northeast Kenya as well as the southwest parts of Uganda and Tanzania. On the other hand, very low AOD values (<0.1) characterized the high precipitation areas (Figure 1(a)) of western and central parts of Kenya, northeast Uganda and southwest of Tanzania during the local wet seasons. The seasonal patterns of AOD over EA are closely associated with the seasonal cycle of precipitation (de Graaf *et al.*, 2010) with the two depicting a more or less inverse relationship between them. The enhanced precipitation during MAM (Figure 1(a)) causes large wet deposition and suppresses emission of aerosols from the ground.

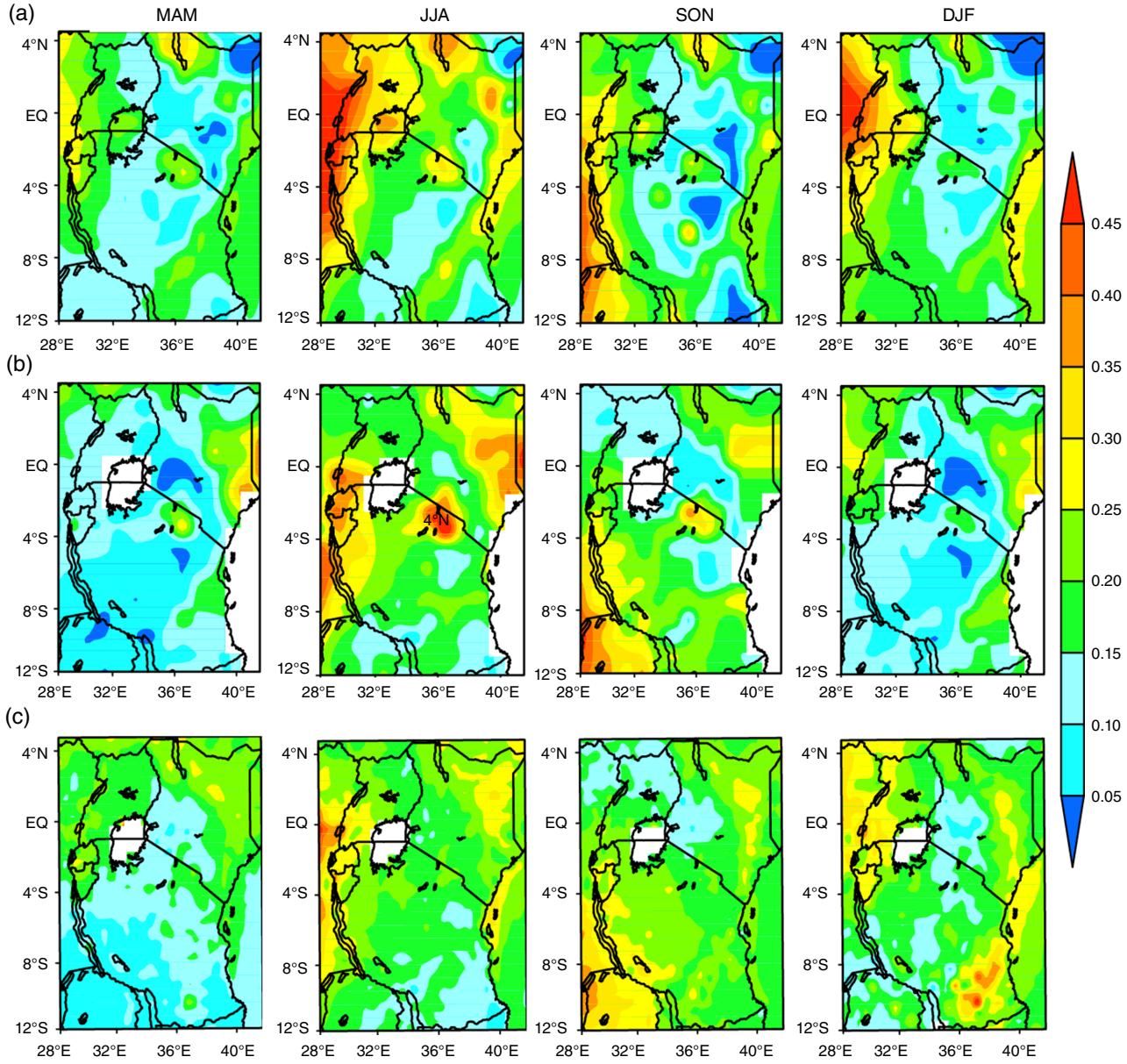

Figure 5. Same as in Figure 4, but for different seasons. [Colour figure can be viewed at wileyonlinelibrary.com].

On the other hand, the enhanced aerosol loading during the local dry seasons could be attributed to increased anthropogenic activities (land preparations, biomass burning and forest fires) which release significant amount of smoke particles into the EA's atmosphere (Ngaina and Muthama, 2014; Makokha *et al.*, 2017). The stronger near-surface winds during JJA over the arid and semi-arid areas of north and eastern parts of Kenya (Figure 1(d)) could accelerate the formation of dust aerosols. The high temperatures in association with strong winds during DJF (Figures 1(b) and (d)) play a crucial role in heating and lifting up loose soil (Boiyo *et al.*, 2017b). This is aggravated by the north easterlies (Figure 1(d)) which transports dust aerosols from the Arabian Peninsula (Gatebe *et al.*, 2001; Boiyo *et al.*, 2017a) to north and eastern parts of the study domain. The enhanced aersosols from aforementioned mechanisms and sources increase backscattering of light resulting in high AODs observed by the sensors during the local dry seasons.

3.3. Seasonality in AOD and association with meteorology

3.3.1. Annual, seasonal and monthly variations of AOD

The 14-year detailed statistics of annual and seasonal mean AOD along with standard deviation and magnitude of inter-annual variability estimated over EA and its constituting countries are presented in Table 1 and Figure 6. The annual averaged AOD values were found to be 0.20 ± 0.01, 0.18 ± 0.01 and 0.20 ± 0.02 as observed by the MODIS Aqua-DT, -DB and MISR, respectively, with the errors indicating temporal heterogeneity. Regarding individual countries, Uganda noticed highest annual mean AOD followed by Kenya and Tanzania (Table 1). Notably, the

enhanced aerosol loading over Uganda and Kenya could be attributed to the fact the two countries are aerosol receptors (Boiyo *et al.*, 2017a). They are located between two aerosol sources: (1) anthropogenic activities in central Africa where biomass burning activities results in significant amount of smoke particles transported to the northern part of EA by the westerlies (Hao and Liu, 1994; Ogwang *et al.*, 2016), (2) natural dust emissions locally produced from the arid and semi-arid lands in north and eastern part of EA, alongside those transported from the Arabian and Saharan Deserts (Gatebe *et al.*, 2001; de Graaf *et al.*, 2010) by north easterlies during certain times of the year (Figure 1(d)). Meanwhile, the daily averaged AODs retrieved by the three sensors over EA and the constituting countries generally showed a single peak distribution of frequencies of occurrences centred at the bin interval 0.1–0.2 (Appendix S1 and Figure S1, Supporting information). This signifies generally a less polluted environment dominated by particular aerosol type.

The seasonally averaged AOD values were noticed to be high (>0.2) during JJA and low (<0.2) during MAM (Table 1 and Figure 6). This pattern was also followed by the constituting countries and is consistent with the results presented in Section 3.2.2. The monthly mean AOD retrieved by the sensors was found to be lower (higher) in March (July) (Figure 6). All the sensors generally observed second AOD trough in November and peak in February. The monthly distribution of AOD for each of the countries was found to be consistent with the regional pattern (Table 1 and Figures 6(b)–(d)). This signifies the role played by individual countries in influencing the regional aerosol load. As aforementioned, the monthly variation in AOD over EA is closely associated with variations in emission sources, anthropogenic activities and seasonal cycles of precipitation. A combination of biomass burning (during December–February and June–July) and dust aerosols (locally derived and due to long-range transport) could enhance the aerosol load during these months (Makokha *et al.*, 2017). The low AOD during March–May and September–November is attributed to large wet deposition (Figure 1(a)) and reduced anthropogenic activities (de Graaf *et al.*, 2010; Boiyo *et al.*, 2017a).

3.3.2. Inter-annual variability and linear trends in AOD

The magnitude of inter-annual variability in AOD was estimated during the entire study period over EA and the constituting countries (Table 1). Overall, AOD values fluctuate from year to year by 5% (as observed by MISR) and ∼6% as observed by DT and DB. The lowest values of inter-annual variability in AOD over EA were the values of ∼6% recorded in Tanzania, with generally low AOD values. However, Kenya and Uganda, with enhanced AOD, had fluctuations ranging between 5 and 9% as observed by different sensors. On seasonal basis, the lowest magnitude of inter-annual variability in AOD occurred during SON over EA, with similar changes (but different magnitudes) observed over each of the countries (Table 1). The highest fluctuation was observed during MAM (for DB and MISR) and DJF for DT with the same pattern (but different magnitudes) consistent over the three countries. Generally, the magnitudes of inter-annual variability in AOD over EA are influenced by changes in emissions and meteorology. There are two major aerosol emission sources over EA: (1) anthropogenic emissions resulting from industrial–vehicular emissions, forest fires, agricultural and biomass burning (Van Vliet and Kinney, 2007; Makokha and Angeyo, 2013; Ngo *et al.*, 2015) and (2) natural dust emissions over the arid and semi-arid areas in north of EA with low (<600 mm year^{-1}) annual rainfall (Figure 1(a)). The meteorological factors (e.g. wind, relative humidity, temperature and precipitation) control production, transport pathway from source to receptor region, exchange between the boundary layer and free troposphere, and removal processes occurring over the source and receptor regions (Panicker *et al.*, 2013; Luo *et al.*, 2014).

It is worth mentioning that AOD values over EA consistently increased during post-2009 (2009–2016) (trend year^{-1} = 0.00279, 0.00221 and 0.00247 for DT, DB and MISR, respectively) as compared to pre-2009 (2002–2008) with respective trends year^{-1} of −0.00148, −0.000387 and −0.00109. In order to detect and quantify this, the percentage (%) variations in trends over EA and each of the countries were analysed during the entire study period, pre-2009 and post-2009 periods (Table 2). During the entire study period, AOD values over EA consistently increased by 0.52, 0.57 and 0.74% year^{-1} as observed by MISR, DT and DB, respectively (significant at 95% represented in red colour and 90% in blue). Furthermore, a significant increase in AOD by 0.95 and 0.58% was observed by DB and MISR, respectively, over Kenya, while Uganda recorded a significant increase of 0.67 and 1.06% observed by DT and DB, respectively. The positive trend in Tanzania was less significant as observed by all the sensors. Except for Kenya, with an insignificant annual increase, a general decrease in AOD trend was observed by the sensors during pre-2009. However, all the sensors observed an increase in AOD trend during post-2009. Meanwhile, the seasonal AOD trends generally increased across the seasons over entire EA and each of constituting countries during the entire study period. This is with the exception of MAM that showed an insignificant negative trend over entire EA, Kenya and Tanzania as observed by DT (Table 2). The trends were high and reliable during the local dry seasons. Specifically, significant trends at 95% (90%) confidence level were observed by DB (MISR) during DJF over EA and 90% confidence level by DB and MISR over Kenya. The overall trends were marked by a general decrease (increase) during pre-2009 (post-2009), with the increase being generally enhanced and significant.

The trends in AOD patterns have been investigated by a number of authors. Negative AOD trends in China have been reported over receptor regions, as positive trends characterize regions overburdened by anthropogenic and natural aerosols sources (Luo *et al.*, 2014; Tan *et al.*, 2015a; Hu *et al.*, 2017). The negative trends over South

Table 1. Regional statistics of AOD for the period 2002–2016 derived from MODIS Aqua (DT, DB) and MISR over EA, Kenya, Uganda and Tanzania.

Sensor	Season	EA		Kenya		Uganda		Tanzania	
		M	MAG	M	MAG	M	MAG	M	MAG
DT	MAM	0.16 ± 0.02	11.77	0.15 ± 0.02	10.62	0.16 ± 0.02	14.14	0.14 ± 0.01	13.25
	JJA	0.23 ± 0.02	12.67	0.22 ± 0.02	18.48	0.31 ± 0.02	14.18	0.21 ± 0.02	12.25
	SON	0.19 ± 0.01	6.78	0.14 ± 0.01	8.95	0.18 ± 0.02	7.85	0.18 ± 0.02	11.46
	DJF	0.21 ± 0.02	13.16	0.13 ± 0.02	16.81	0.21 ± 0.03	16.01	0.18 ± 0.02	15.45
	Annual	0.20 ± 0.01	5.84	0.16 ± 0.02	8.51	0.22 ± 0.02	7.04	0.18 ± 0.02	6.45
DB	MAM	0.12 ± 0.01	12.74	0.16 ± 0.02	10.21	0.12 ± 0.02	17.46	0.10 ± 0.01	14.77
	JJA	0.22 ± 0.02	9.82	0.24 ± 0.02	13.54	0.29 ± 0.01	13.14	0.22 ± 0.02	9.92
	SON	0.21 ± 0.02	7.51	0.18 ± 0.02	8.42	0.14 ± 0.02	9.76	0.22 ± 0.03	9.43
	DJF	0.15 ± 0.01	10.17	0.16 ± 0.01	7.26	0.15 ± 0.02	13.18	0.12 ± 0.02	14.52
	Annual	0.18 ± 0.01	6.02	0.19 ± 0.02	7.35	0.15 ± 0.02	13.18	0.17 ± 0.01	6.37
MISR	MAM	0.15 ± 0.02	6.03	0.17 ± 0.01	7.83	0.17 ± 0.01	13.84	0.12 ± 0.02	13.67
	JJA	0.21 ± 0.02	9.32	0.22 ± 0.02	12.13	0.22 ± 0.02	12.25	0.17 ± 0.02	9.95
	SON	0.22 ± 0.01	5.42	0.19 ± 0.02	6.22	0.17 ± 0.01	7.32	0.21 ± 0.01	7.66
	DJF	0.21 ± 0.02	10.81	0.18 ± 0.02	6.83	0.22 ± 0.02	16.27	0.20 ± 0.02	12.46
	Annual	0.20 ± 0.02	5.02	0.19 ± 0.02	4.84	0.20 ± 0.01	5.77	0.18 ± 0.02	6.45

The symbols M ($\pm\sigma$) and MAG refers to the mean ($\pm$standard deviation) and magnitude of inter-annual variability (in %), respectively. The AODs corresponding to MODIS Aqua (DT, DB) and MISR are derived at 500 and 555 nm, respectively.

Table 2. Annual and seasonal percentage (%) variations in trends per year of AOD derived from MODIS Aqua (DT, DB) and MISR during entire period (2002–2016), pre-2009 (2002–2009) and post-2009 (2009–2016) over EA.

	Annual			MAM			JJA			SON			DJF		
	DT	DB	MISR	DT	DB	MISR	DT	DB	MISR	DT	DB	MISR	DT	DB	MISR
Entire period															
EA	*0.57*	**0.74**	*0.52*	−0.4	0.48	0.19	0.98	0.76	0.61	0.38	0.52	0.20	0.90	**1.15**	**1.16**
Kenya	0.60	**0.95**	**0.58**	−0.7	0.58	0.28	1.42	1.22	1.59	0.56	**0.70**	0.27	0.77	*1.12*	*0.73*
Uganda	*0.68*	**1.06**	0.43	0.17	1.31	0.63	0.48	0.66	0.12	*0.83*	1.4	0.05	0.75	0.97	0.92
Tanzania	0.19	0.48	0.41	−0.9	0.2	0.16	0.73	0.38	0.45	0.12	0.23	0.17	0.46	1.23	0.88
Pre-2009															
EA	−0.2	−0.2	−0.6	0.59	**2.44**	0.96	−0.04	−0.01	−0.01	**−0.7**	**−1.1**	−0.5	−1.1	−1.4	−0.3
Kenya	0.72	0.84	0.27	0.01	2.73	0.79	0.05	*0.07*	0.09	1.44	**−0.4**	0.35	0.96	−0.3	**−2.0**
Uganda	−0.6	0.17	−1	1.52	3.57	3.52	−0.2	−0.1	−0.1	1.37	**4.09**	1.42	−1.9	−2.7	**−6.1**
Tanzania	−1.4	−1	−0.9	0.08	1.58	0.76	−0.03	−0.02	0.01	−2.4	−2.4	−1.4	−2.4	−1.5	**−2.7**
Post-2009															
EA	**1.82**	1.23	*1.22*	0.87	1.14	1.23	0.71	**0.42**	**0.05**	−0.1	0.17	**−0.5**	**3.64**	**3.62**	**3.8**
Kenya	0.27	0.32	−0.0	−0.7	−0.0	0.20	0.57	**0.18**	−0.4	−1.0	**−0.4**	**−0.6**	1.96	**1.82**	*1.55*
Uganda	1.26	1.36	1.19	0.28	1.66	0.98	0.71	**0.5**	−1.1	−0.2	0.32	0.97	**3.48**	**3.06**	*3.77*
Tanzania	*1.58*	*1.56*	**1.66**	1.03	1.76	*2.56*	0.21	**0.23**	0.03	−0.3	−0.1	−0.8	**4.66**	**5.67**	**4.59**

The numerals in bold are significant at 95% confidence level, whereas those in italic are significant at 90% confidence, and the rest are less significant.

Korea were attributed to reduced emissions of pollutants from factories and implementation of advanced technologies that minimizes particle emissions (Panicker *et al.*, 2013). Similar variations in trends have been reported over different regions of SA (Kumar *et al.*, 2014a, 2015; Adesina *et al.*, 2016), where negative trends were attributed to the strict implementation of suitable environmental protection policies aimed at reducing particulate matter emissions.

In the present study, the negative trends observed during pre-2009 (though insignificant) interprets that EA experienced low AOD attributed to lower population (by then), characterized by reduced anthropogenic activities, shrunken economic growth and sparse industries (Makokha *et al.*, 2017; Boiyo *et al.*, 2017a). In contrast, increasing AOD trends during the entire period and post-2009 indicates an increase in the aerosol loading attributed to: (1) population growth leading to increased anthropogenic activities (Gatebe *et al.*, 2001; Ngaina and Muthama, 2014), (2) industrialization resulting to increased anthropogenic emissions (Mabasi, 2009; Ngo *et al.*, 2015) and (3) climate change occasioned by increased temperature and reduced precipitation (Yang *et al.*, 2015; Kerandi *et al.*, 2017). These results in increased photochemical processes with reduced deposition and increased emission of dust aerosols from the arid and semi-arid regions of EA. As previously mentioned, the enhanced positive trends during local dry seasons are consistent with seasonal cycles of emission sources, transport pathways and modulations induced by local meteorological conditions. However, the decreasing trends observed by DT during MAM (though insignificant) are closely

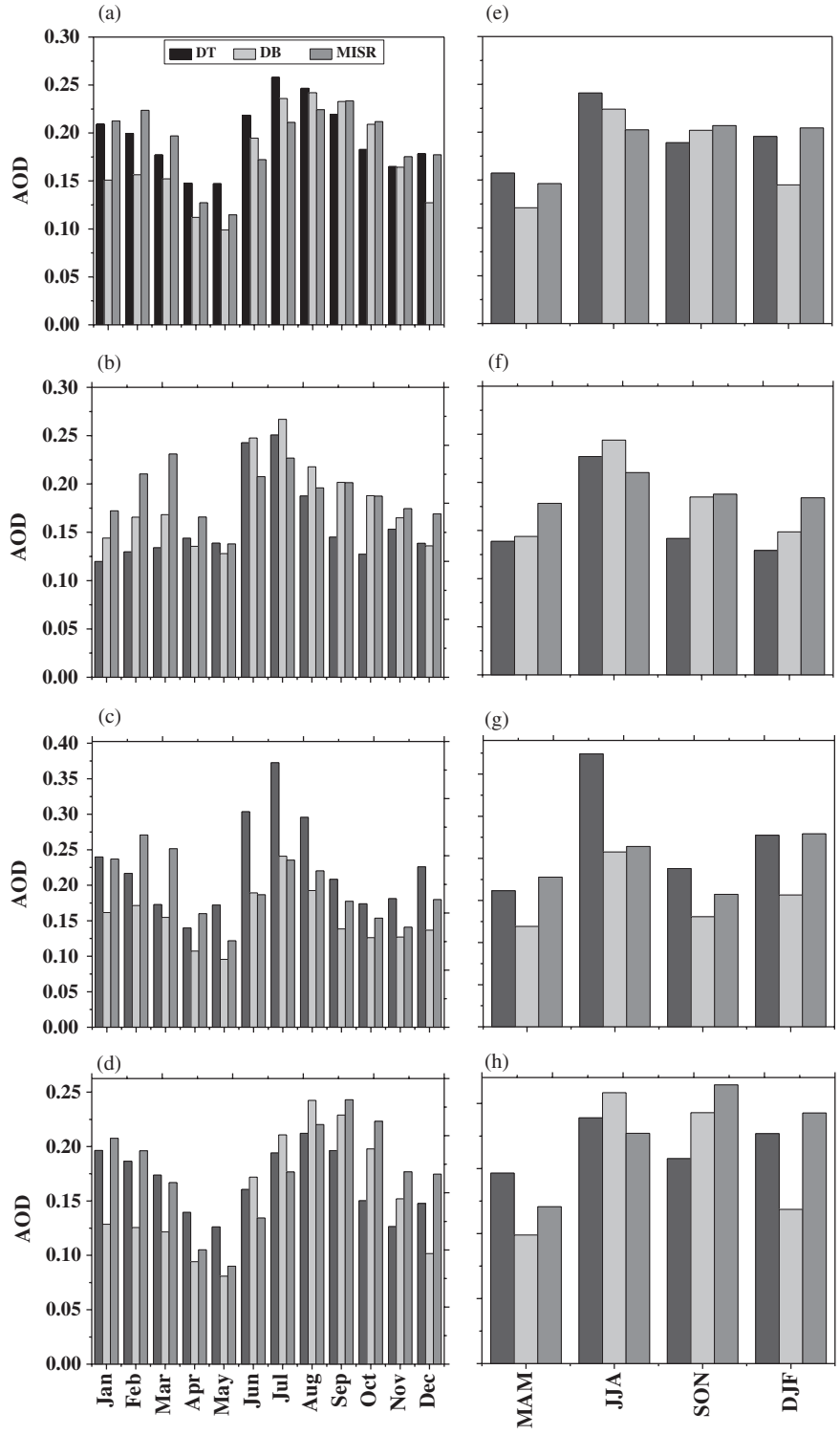

Figure 6. Monthly (a–d) and seasonal (e–h) mean variations of AOD observed over entire EA (a, e), Kenya (b, f), Uganda (c, g) and Tanzania (d, h) during the study period.

associated with seasonal cycles of precipitation and anthropogenic activities.

3.3.3. Association between the trends in AOD and meteorology

In order to establish a potential association between trends in AOD and regional meteorology, the trends in four important meteorological parameters, i.e. temperature, wind speed, relative humidity and precipitation over EA and each of the individual countries were investigated during the study period. The study relied solely on the relationships between AOD trends and those of the meteorological parameters. However, deeper insights into the causality between the observables as well as the role of

atmospheric transport will be investigated in our future modelling studies. A rise in temperature is supposed to intensify surface heating resulting to increased convection hence higher aerosol loading. Higher temperatures and relative humidity during dry periods intensify hygroscopic growth of aerosols and gas-to-particle conversion process. This in turn produces more secondary aerosols resulting in high AOD (Tan *et al.*, 2015b; Floutsi *et al.*, 2016; Kang *et al.*, 2016). Temperature over EA and each of the constituting countries showed a significant increase (Figure 7(a)) during the entire study period, suggesting that changes in temperature could facilitate additional input of aerosol in the atmosphere. On the other hand, wind speed bears a decisive role in transporting aerosols from source to receptor regions. A decline in wind speed could weaken the transport of aerosols leading to increasing (decreasing) AOD trends over the source (receptor) regions (Luo *et al.*, 2014; Tan *et al.*, 2015a). Generally, the positive AOD trends observed over EA could be connected to the decline in surface winds (Figure 7(b)) which leads to more accumulation of aerosols in the source regions.

Besides, high temperatures and RH intensifies gas-to-particle conversion processes resulting in elevated concentration of fine-mode aerosols (Kumar *et al.*, 2015; Kang *et al.*, 2016). Trends in RH (Figure 7(c)) over EA and the constituting countries generally decreased with increase in an aerosol load, indicating that the RH growth of AOD was less significant during the study period. Furthermore, precipitation can affect the aerosol burden especially dust through several mechanisms: (1) precipitation scavenging removes aerosol particles from the atmosphere lowering its concentration; (2) it increases soil moisture suppressing wind-induced dust emissions from the ground and (3) fosters vegetation growth, which could further inhibits dust emissions. Hence, trends in precipitation could explain trends in AOD over EA. Precipitation over EA and each of the individual countries showed a significant decrease (Figure 7(d)) which is consistent with investigations by a number of authors including Liebmann *et al.* (2014), Maidment *et al.* (2015) and Ongoma and Chen (2017). As trends in precipitation showed inverse pattern to those in AOD, it may be implied that reduced precipitation could be responsible for the observed aerosol load and vice versa. In addition to regional meteorology, changes in local emissions and sources could interpret escalating AOD over EA and should be a subject of future research.

3.4. Spatial trends and tendencies in AOD

The linear trend analysis based on domain averaged AOD (Section 3.2.2) revealed an upwards AOD trend over EA. In order to detect and identify specific locations with positive and negative trends leading to the observed overall trends, pixel-wise AOD trends and relative changes (tendencies) were computed, with the former evaluated at 90% confidence level. The computed AOD tendencies unravel existence of any prominent changes in the overall aerosol loading during the first (2002–2008) or second half (2009–2016) halves of the 14-year study period. The changes could be different from the corresponding AOD trends, which refers to continuous time series (Mehta, 2015). The spatial distribution of annual AOD trends retrieved from DT, DB and MISR is shown in Figures 8(a)–(c), respectively, while Figures 10(a)–(c) shows the respective tendencies observed over EA. Comparing the patterns of variation in trends and tendencies with the average annual and seasonal AOD distribution (Figures 4 and 5), it is revealed that positive (negative) trends generally correspond to high (low) AOD centres, further signifying the role of emission sources in enhancing AOD distribution over EA.

An overall increase in annual AOD trends and tendencies was observed over most regions in Kenya and Uganda except, southwest of the respective countries. The trends and tendencies were higher (>0.002 and >0.2 year^{-1}, respectively) and significant over the arid and semi-arid areas of northern parts of EA dominated by dust. Positive AOD trends and tendencies also dominated over most parts of Kenya as observed by DB, being relatively high and significant over western and northeast parts of Kenya. Furthermore, MISR noticed significant positive trends over western parts of Kenya. On a seasonal basis, positive trends and tendencies (Figures 9(a)–(c) and 11(a)–(c)) dominated most of EA's domain in all seasons except MAM with prevailing 'long rains' (Figure 1(a)). The magnitude of negative trends and changes noticed during MAM were more pronounced as observed by the MODIS Aqua-DT followed by MISR. Across all seasons, the trends were relatively high and significant over north part of EA as observed by the three sensors.

The observed positive trends in most parts of EA imply an increase in aerosol load, whereas negative trends interpret reduced load. As outlined in Section 3.2.2, the magnitudes and signs of trends and relative changes are influenced by both emission and meteorological factors. EA is experiencing an overall increase in temperature accompanied by reduced precipitation and wind speed (Indeje *et al.,* 2000; Yang *et al.*, 2015), conditions favourable for increased aerosol emmisions. The positive trends over arid and semi-arid regions of northern part of EA could be associated with reduced precipitation (Figure 1(a)) resulting to an increase in locally generated dust (Gatebe *et al.*, 2001; Ngaina and Muthama, 2014), while those observed in the border regions with DRC could be due to intense biomass burning activities (Hao and Liu, 1994; de Graaf *et al.*, 2010). In addition to this, local anthropogenic activities arising from biomass burning and industrial–vehicular emissions (Kinney *et al.*, 2011; Makokha and Angeyo, 2013; Ngo *et al.*, 2015) could interpret the increasing AOD trends over EA. On the other hand, negative trends observed during MAM are associated with large wet deposition of aerosols resulting from the seasonal cycles of precipitation (de Graaf *et al.*, 2010; Makokha *et al.*, 2017).

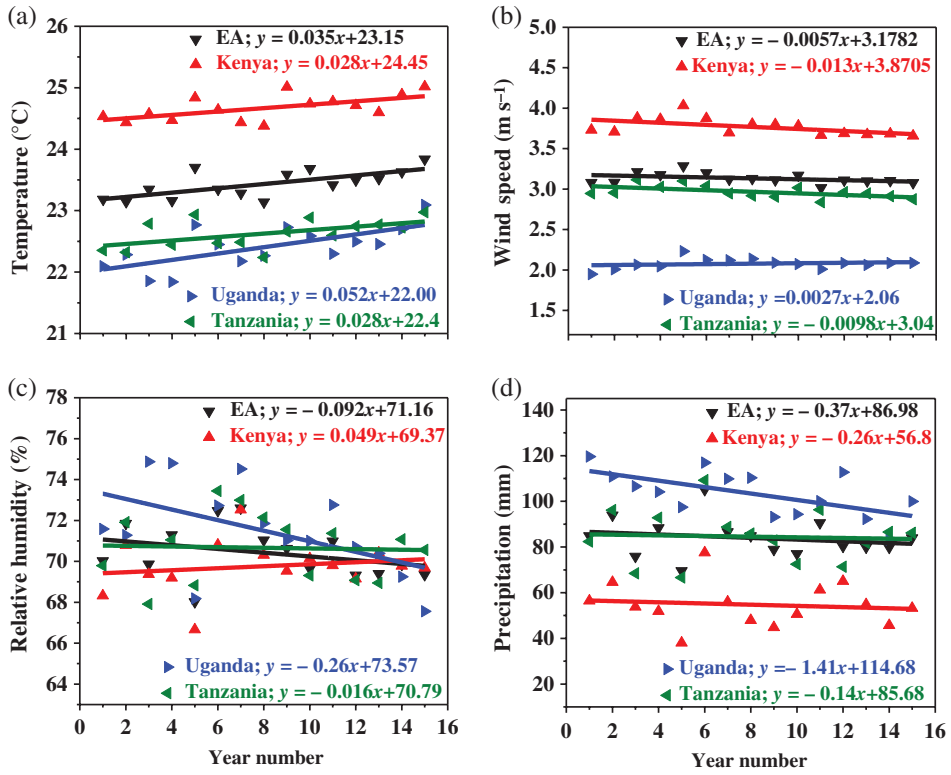

Figure 7. Annual trends observed in various meteorological parameters: (a) temperature, (b) wind speed, (c) relative humidity and (d) precipitation over entire EA and each of the countries. The straight lines correspond to the linear fitting and the regression equation is also given in all panels. [Colour figure can be viewed at wileyonlinelibrary.com].

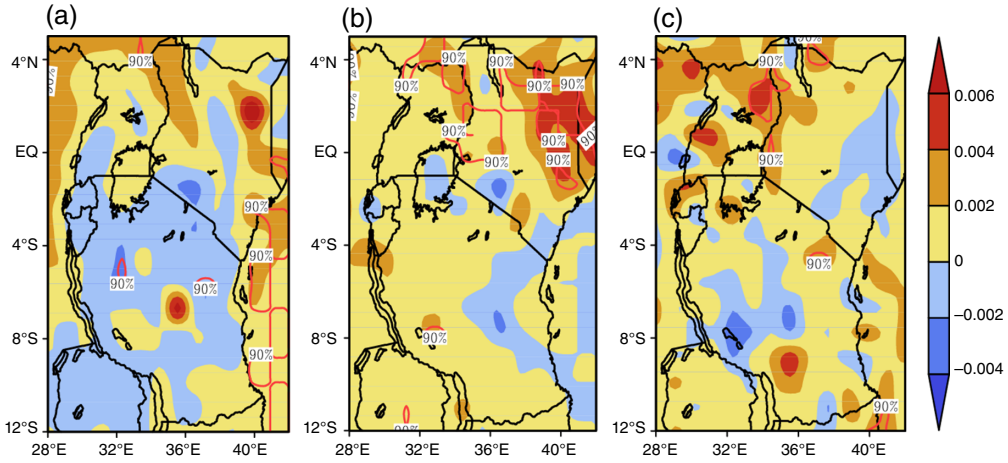

Figure 8. Spatial distribution of annual trends in AOD derived from (a) MODIS Aqua-DT, (b) MODIS Aqua-DB and (c) MISR in the units of year^{-1}. The shadings shows the sign and magnitude of trend, while the confidence levels are also shown as numerals embedded on contours. [Colour figure can be viewed at wileyonlinelibrary.com].

3.5. Aerosol discrimination process

In order to investigate the dominant aerosol type over selected cities in EA, the AOD_{550} *versus* $AE_{470–660}$ scatter diagrams were constructed using the threshold values outlined in Section 3.3.1. Generally, CCB aerosols type presented the largest number of cluster points, followed by BUI and MXD aerosol types, whereas CMA and DDT showed the least (Figure 12). The percentage contributions of each of the four different types of aerosols noticed over the three locations are also shown in all the panels in Figure 12. During the study period, CCB was the dominant aerosol type constituting 75.71, 74.38 and 73.32% over Nairobi, Kampala and Dodoma, respectively. The respective contribution from CMA (0.38, 0.07 and 0.52%) and DDT (1.46, 0.07 and 1.57%) were limited due to their large proximity from the ocean and deserts. Also, the enhanced precipitation (Figure 1(a)) caused large wet deposition of aerosols as well as suppressing emission of dust particles from the ground. The influence of BUI aerosol type was significant with contributions of 7.25, 9.97

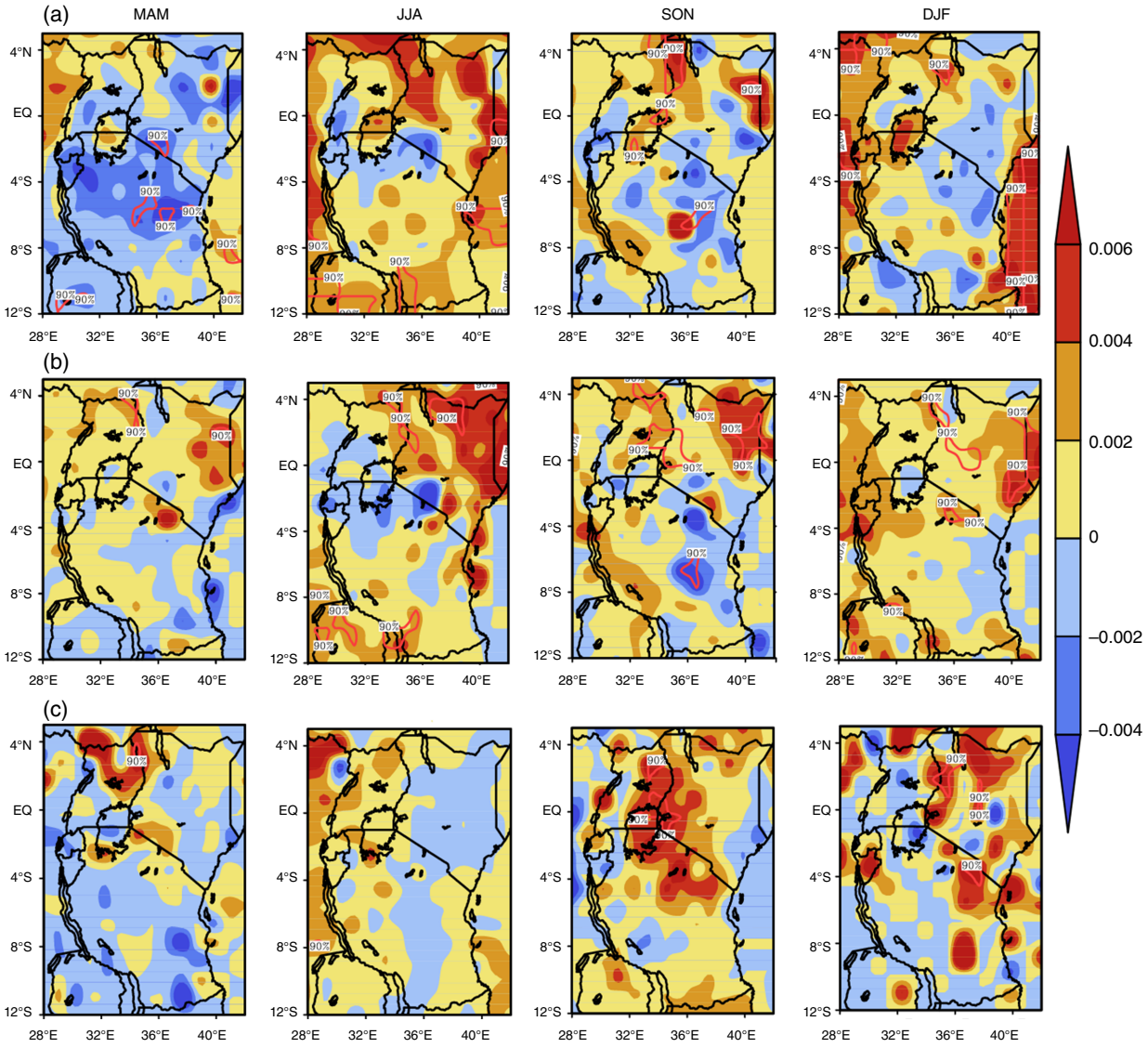

Figure 9. Same as in Figure 8, but for the seasonally averaged spatial trends in AOD. [Colour figure can be viewed at wileyonlinelibrary.com].

and 6.84% over Nairobi, Kampala and Dodoma, respectively. This is attributed to the fact that the three locations considered are highly urbanized and dominated by industrial–vehicular emissions (Kinney *et al.*, 2011; Ngo *et al.*, 2015; Makokha *et al.*, 2017). They are also closer to major agricultural zones where frequent crop-residue burning occurs (Mabasi, 2009; Makokha and Angeyo, 2013). Notably, the influence of MXD aerosol type was significant contributing to 15.22, 15.65 and 17.78% over Nairobi, Kampala and Dodoma. In summary, it is worth mentioning that the averaged contribution of each of the five aerosol types over the three locations in EA during the study period were sequenced from high to low as CCB (74.47%), MXD (16.22%), BUI (8.02%), DDT (1.03%) and CMA (0.32%).

4. Summary and conclusions

Using 14 years (2002–2016) of Level 3 aerosol data sets retrieved from three algorithms (MODIS Aqua-DT, DB and MISR), this study presented an in-depth understanding of spatio-temporal distribution and trends in AOD over EA as well as examined the consistency and differences between the data sets. An inter-comparison between AODs retrieved by different algorithms over EA noticed highest correlation between DT and DB ($r = 0.87$), followed by MISR and DB ($r = 0.76$), and least for MISR and DT ($r = 0.72$). The AODs retrieved from the algorithms revealed significant positive correlations with moderate (>0.5–0.8) to high (≥0.8) correlations dominating the study domain, whereas a few regions exhibited low (0–0.5) positive correlations. The spatial patterns of annual mean AOD observed over EA were generally characterized by low (<0.2), moderate (0.2–0.35) and high (>0.35) areas. Low AODs were observed by the sensors in the high altitude and densely vegetated regions over western and central parts of Kenya and central Tanzania. Moderate AOD values were found over the dust dominant arid and semi-arid zones of the north part of EA. A single peak distribution of AOD frequency of occurrences were

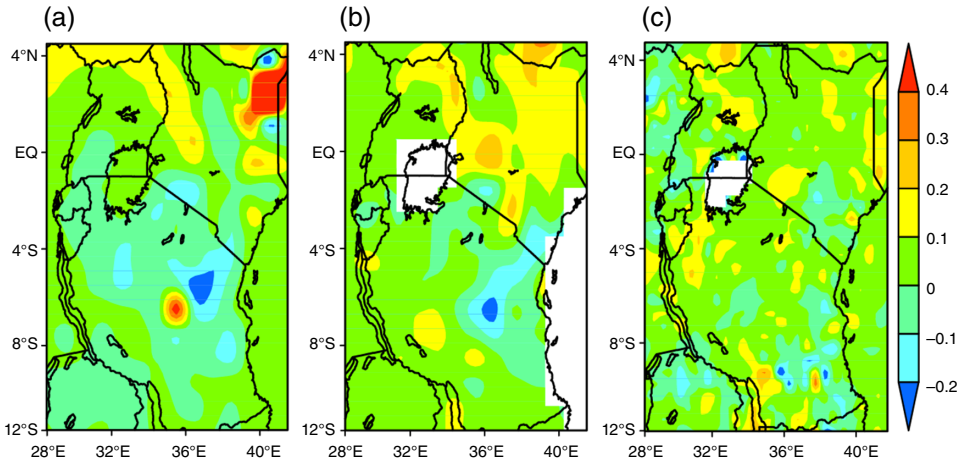

Figure 10. Same as in Figure 4, but for the spatial distribution of relative changes in annual mean AOD. [Colour figure can be viewed at wileyonlinelibrary.com].

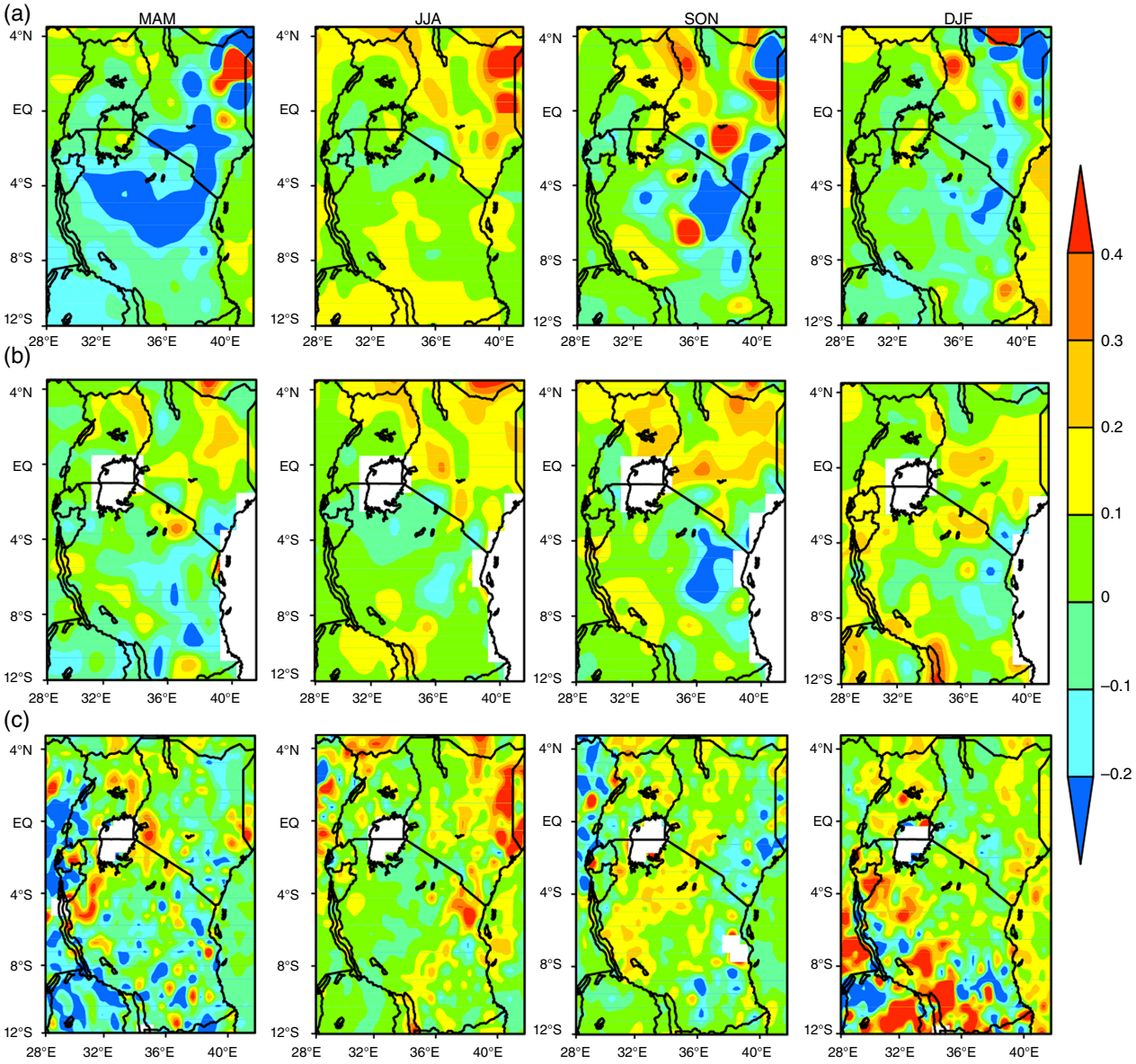

Figure 11. Same as in Figure 10, but for different seasons. [Colour figure can be viewed at wileyonlinelibrary.com].

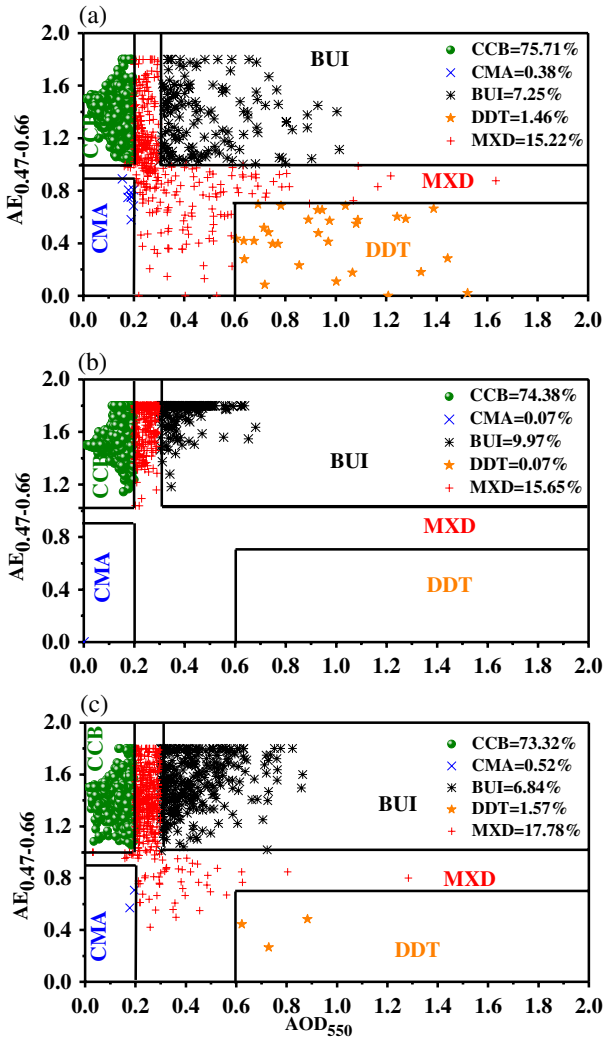

Figure 12. Scatter plots of $AE_{0.47-0.66}$ *versus* AOD_{550} derived MODIS Aqua-DT for the identification of dominant aerosol types over three representative cities in EA: (a) Nairobi, (b) Kampala, (c) Dodoma during the study period. The labels stand for CMA: clean maritime aerosol type, CCB: continental clean background type, BUI: biomass burning and urban/industrial type, DDT: desert dust type and MXD: mixed type of aerosols. The percentage contribution of each aerosol type is also shown in all the panels. [Colour figure can be viewed at wileyonlinelibrary.com].

observed over EA and each of the constituting countries signifying a less polluted environment dominated by a particular aerosol type. The seasonal AOD climatologies over the entire study domain were consistent with that of the annual patterns, being low during the local wet seasons and high during the local dry seasons. This has been attributed to seasonality in emission sources, anthropogenic activities and modulations induced by regional meteorological factors such as temperature, relative humidity, wind speed and precipitation.

Analysis of AOD trends over EA during 2002–2016 showed a significant increase by 0.52, 0.57 and 0.74% $year^{-1}$ as detected by the MISR, DT and DB, respectively. Positive AOD trends dominated during the local dry seasons, being more pronounced during JJA over the dust dominant regions north of EA. On the other hand, negative trends characterized the local wet season (mainly MAM) attributed to large wet deposition process. The trends in aerosol loading were well aligned with those in meteorological parameters: increasing with rise in temperature, decrease in wind speed and decrease in precipitation. It was later revealed that CCB (74.47%) was the dominant aerosol type over selected cities in EA. Other aerosol types made contributions sequenced from high to low as MXD (16.22%), BUI (8.02%), DDT (1.03%) and CMA (0.32%).

This work conclusively compared spatial variations and trends in AOD retrieved from three different algorithms over EA. Despite variations in the emphasis that each algorithm places on the strength of AOD, no critical differences between the data sets were detected over EA. The data sets showed close resemblance in most aspects, except a few cases where either of the algorithms failed owing to limitations imposed by the algorithm to the underlying surface types. It is, therefore, evident that either of the algorithms could be well suited for qualitative and quantitative aerosol related studies over EA. However, based on this work and our recent investigation (Boiyo *et al.*, 2017b), MODIS Aqua-DT could be well suited to characterize AOD over the most locations of EA. The present work has also outlined a possible link between trends in AOD and those in meteorological parameters. Notably, the change in emission has a potential effect of adversely affecting AOD trends over EA. In order to investigate this in details, revealing the causal relationship, a modelling study is planned as a future research project over EA.

Acknowledgements

This work was financially supported by the National Key R and D Program Pilot Projects of China (grant no. 2016YFC0203304), the National Natural Science Foundation of China (grant no. 91644224) and the NUIST Key Laboratory for Aerosol-Cloud-Precipitation of China Meteorological Administration (grant no. KDW1404). The authors are thankful to the NASA LAADS and GIOVANNI online analysis and visualization system for providing and processing various satellite data sets utilized. The meteorological data used in this work were procured from the ECMWF ERA-Interim reanalysis, Climate Research Unit (CRU) and TRMM. The first author Mr Richard Boiyo extends sincere gratitude to Ministry of Higher Education, Science and Technology of Kenya, Meru University of Information Science and Technology (Kenya), China Scholarship Council (China) and Nanjing University of Information Science and Technology (China) for facilitating his 3-year PhD scholarship (2015–2018). We thank Prof. Radan Huth, Editor-in-Chief and Dr Ian McKendry, Associate Editor of the journal; and the three anonymous reviewers for their helpful comments and constructive suggestions towards the improvement of earlier versions of the manuscript. The authors declare that there is no conflict of interest on the publication of this work.

Supporting information

The following supporting information is available as part of the online article:

Appendix S1. Frequency distributions of AOD.

Figure S1. Annual relative frequency of occurrences (in %) of AOD over (a) EA, (b) Kenya, (c) Uganda and (d) Tanzania obtained from the MODIS Aqua DT, DB and MISR during the study period. The black solid, dashed and dotted lines corresponds to the Gaussian curves fitted to the obtained distribution for MODIS Aqua DT, DB and MISR sensors, respectively.

References

Adesina AJ, Kumar KR, Sivakumar V, Piketh SJ. 2016. Intercomparison and assessment of long-term (2004–2013) multiple satellite aerosol products over two contrasting sites in South Africa. *J. Atmos. Sol. Terr. Phys.* **148**: 82–95. https://doi.org/10.1016/j.jastp.2016.09.001.

Adesina AJ, Piketh S, Kumar KR, Venkataraman S. 2017. Characteristics of columnar aerosol optical and microphysical properties retrieved from the sun photometer and its impact on radiative forcing over Skukuza (South Africa) during 1999–2010. *Environ. Sci. Pollut. Res.* **24**: 16160–16171. https://doi.org/10.1007/s11356-017-9211-2.

Alam K, Qureshi S, Blaschke T. 2011. Monitoring spatio-temporal aerosol patterns over Pakistan based on MODIS, TOMS and MISR satellite data and a HYSPLIT model. *Atmos. Environ.* **45**: 4641–4651. https://doi.org/10.1016/j.atmosenv.2011.05.055.

Albrecht BA. 1989. Aerosols, cloud microphysics, and fractional cloudiness. *Science* **245**: 1227–1230.

Alpert P, Shvainshtein O, Kishcha P. 2012. AOD trends over megacities based on space monitoring using MODIS and MISR. *Am. J. Clim. Change* **1**: 117–131. https://doi.org/10.4236/ajcc.2012.13010.

Amiridis V, Balis DS, Kazadzis S, Bais A, Giannakaki E, Papayannis A, Zerefos C. 2005. Four-year aerosol observations with a Raman lidar at Thessaloniki, Greece, in the framework of European Aerosol Research Lidar Network (EARLINET). *J. Geophys. Res. Atmos.* **110**: D21203. https://doi.org/10.1029/2005JD006190.

Ångström A. 1961. Techniques of determining the turbidity of the atmosphere. *Tellus A* **13**: 214–223. https://doi.org/10.1111/j.2153-3490.1961.tb00078.

Bennouna YS, Cachorro VE, Toledano C, Berjón A, Prats ND, Fuertes R, Gonzalez Rodrigo R, Torres B, De Frutos AM. 2011. Comparison of atmospheric aerosol climatologies over southwestern Spain derived from AERONET and MODIS. *Remote Sens. Environ.* **115**: 1272–1284. https://doi.org/10.1016/j.rse.2011.01.011.

Bibi H, Alam K, Bibi S. 2016. In-depth discrimination of aerosol types using multiple clustering techniques over four locations in Indo-Gangetic Plains. *Atmos. Res.* **181**: 106–114. https://doi.org/10.1016/j.atmosres.2016.06.017.

Boiyo R, Kumar KR, Zhao T, Bao Y. 2017a. Climatological analysis of aerosol optical properties over East Africa observed from space-borne sensors during 2001–2015. *Atmos. Environ.* **152**: 298–313. https://doi.org/10.1016/j.atmosenv.2016.12.050.

Boiyo R, Kumar KR, Zhao T. 2017b. Statistical intercomparison and validation of multisensory aerosol optical depth retrievals over three AERONET sites in Kenya, East Africa. *Atmos. Res.* **197**: 277–288. https://doi.org/10.1016/j.atmosres.2017.07.012.

Charlson RJ, Schwartz SE, Hales JM, Cess RD, Coakley JA, Hansen JE, Hofmann DJ. 1992. Climate forcing by anthropogenic aerosols. *Science* **255**: 423–430. https://doi.org/10.1126/science.255.5043.423.

Che H, Zhang Y, Chen H, Damiri B, Goloub P, Li Z, Zhang X, Wei Y, Zhou H, Dong F, Li D, Zhou T. 2009. Instrument calibration and aerosol optical depth validation of the China aerosol remote sensing network. *J. Geophys. Res*. **114**: D03206. https://doi.org/10.1029/2008JD011030.

Dahutia P, Pathak B, Bhuyan PK. 2017. Aerosols characteristics, trends and their climatic implications over northeast India and adjoining South Asia. *Int. J. Climatol.* https://doi.org/10.1002/joc.5240.

Diner DJ, Abdou WA, Bruegge CJ, Conel JE, Crean KA, Gaitley BJ, Helmlinger MC, Kahn RA, Martonchik JV, Pilorz SH, Holben BN. 2001. MISR aerosol optical depth retrieval over southern Africa during the SAFARI-2000 dry season campaign. *Geophys. Res. Lett*. **28**: 3127–3130. https://doi.org/1029/2001GL013188.

Egondi T, Muindi K, Kyobutungi C, Gatari M. 2016. Measuring exposure levels of inhalable airborne particles ($PM_{2.5}$) in two socially deprived areas of Nairobi, Kenya. *Environ. Res.* **148**: 500–506. https://doi.org/10.1016/j.envres.2016.03.018.

Floutsi AA, Korras-Carraca MB, Matsoukas C, Hatzianastassiou N, Biskos G. 2016. Climatology and trends of aerosol optical depth over the Mediterranean Basin during the last 12 years (2002–2014) based on collection 006 MODIS aqua data. *Sci. Total Environ.* **551–552**: 292–303. https://doi.org/10.1016/j.scitotenv.2016.01.192.

Gatebe CK, Tyson PD, Annegarn HJ, Helas G, Kinyua AM, Piketh SJ. 2001. Characterization and transport of aerosols over equatorial eastern Africa. *Global Biogeochem. Cycles* **15**: 663–672. https://doi.org/10.1029/2000GB001340.

Gautam R, Hsu NC, Lau WK-M, Yasunari TJ. 2013. Satellite observations of desert dust-induced Himalayan snow darkening. *Geophys. Res. Lett.* **40**: 988–993. https://doi.org/10.1002/grl.50226.

de Graaf TM, Aben LG, Stammes IP. 2010. Satellite observations of the seasonal cycles of absorbing aerosols in Africa related to the monsoon rainfall. *Atmos. Environ.* **4410**: 1274–1283. https://doi.org/10.1016/j.atmosenv.2009.12.038.

Guleria RP, Kuniyal JC, Rawat PS, Thakur HK, Sharma M, Sharma NL, Dhyani PP, Singh M. 2012a. Validation of MODIS retrieval aerosol optical depth and an investigation on aerosol transport over Mohal in the northwestern Indian Himalaya. *Int. J. Remote Sens.* **33**: 5379–5401. https://doi.org/10.1080/01431161.2012.657374.

Guleria RP, Kuniyal JC, Dhyani PP. 2012b. Validation of space-born moderate resolution imaging spectroradiometer remote sensors aerosol products using application of ground-based multi-wavelength radiometer. *Adv. Space Res.* **50**: 1391–1404. https://doi.org/10.1016/j.asr.2012.07.002.

Guleria RP, Kuniyal JC, Joshi N, Dhyani PP, Sharma NL. 2014. Impact of aerosol on surface reaching solar irradiance over Mohal in the northwestern Himalaya, India. *J. Atmos. Sol. Terr. Phys.* **108**: 41–49. https://doi.org/10.1016/j.jastp.2013.12.002.

Hao WM, Liu MH. 1994. Spatial and temporal distribution of tropical biomass burning. *Global Biogeochem. Cycles* **8**: 495–503. https://doi.org/10.1029/94GB02086.

Harris I, Jones PD, Osborn TJ, Lister DH. 2014. Updated high-resolution grids of monthly climatic observations – the CRU TS3.10 dataset. *Int. J. Climatol.* **34**: 623–642. https://doi.org/10.1002/joc.3711.

Haywood JM, Boucher O. 2000. Estimates of the direct and indirect radiative forcing due to tropospheric aerosols: a review. *Rev. Geophys.* **38**: 513–543.

Holben BN, Eck TF, Slutsker I, Tanré D, Buis JP, Setzer A, Vermote E, Reagan JA, Kaufman YJ, Nakajima T, Lavenu F, Jankowiak I, Smirnov A. 1998. AERONET – a federated instrument network and data archive for aerosol characterization. *Remote Sens. Environ*. **66**: 1–16. https://doi.org/10.1016/S0034-425700031-5.

Hsu NC, Tsay SC, King MD, Herman JR. 2004. Aerosol properties over bright-reflecting source regions. *IEEE Trans. Geosci. Remote Sens.* **42**: 557–569.

Hsu NC, Tsay SC, King MD, Jay RH. 2006. Deep Blue retrievals of Asian aerosol properties during ACE-Asia. *IEEE Trans. Geosci. Remote Sens.* **44**: 3180–3195.

Hsu NC, Jeong M-J, Bettenhausen C, Sayer AM, Hansell R, Seftor CS, Huang J, Tsay S-C. 2013. Enhanced Deep Blue aerosol retrieval algorithm: the second generation. *J. Geophys. Res.* **118**: 9296–9315. https://doi.org/10.1002/jgrd.50712.

Hu K, Kumar KR, Kang N, Boiyo R, Wu J. 2017. Spatial-temporal characteristics of aerosols and changes in trends over China with recent MODIS collection 6 satellite data. *Environ. Sci. Pollut. Res.* https://doi.org/10.1007/s11356-017-0715-6.

Huang Y, Dickinson RE, Chameides WL. 2006. Impact of aerosol indirect effect on surface temperature over East Asia. *Proc. Natl. Acad. Sci. U.S.A.* **103**: 4371–4376. https://doi.org/10.1073/pnas.0504428103.

Huffman GJ, Bolvin DT, Nelki EJ, Wolff DB, Adler RF, Gu G, Hong Y, Bowman KP, Stocker EF. 2007. The TRMM multisatellite precipitation analysis (TMPA): quasi-global, multiyear, combined-sensor precipitation estimates at fine scales. *J. Hydrometeorol.* **8**: 38–55. https://doi.org/10.1175/JHM560.1.

Ignatov A, Sapper J, Cox S, Laszlo I, Nalli NR, Kidwell KB. 2004. Operational aerosol observations (AEROBS) from AVHRR/3 on board NOAA-KLM satellites. *J. Atmos. Oceanic Technol.* **21**: 3–26. https://doi.org/10.1175/1520-0426.

Indeje M, Semazzi FHM, Ogallo LJ. 2000. ENSO signals in East African rainfall seasons. *Int. J. Climatol.* **20**: 19–46. https://doi.org/10.1002/(sici)1097-0088(200001).

IPCC. 2013. In *Climate Change 2013: The Physical Science Basis. Contribution of Working Group I to the Fifth 4 Assessment Report*

of the Intergovernmental Panel on Climate Change, Stocker TF, Qin D, Plattner G-K, Tignor M, Allen SK, Boschung J, Nauels A, Xia Y, Bex V, Midgley PM (eds). Cambridge University Press: Cambridge, UK and New York, NY, 1535. https://doi.org/10.1017/CBO9781107415324.

Kahn RA, Barbara JG, Garay MJ, Diner DJ, Eck TF, Smirnov A, Holben BN. 2010. Multiangle imaging spectroradiometer global aerosol product assessment by comparison with the aerosol robotic network. *J. Geophys. Res. Atmos.* **115**: D23209. https://doi.org/10.1029/2010jd014601.

Kang N, Kumar KR, Hu K, Yu X, Yin Y. 2016. Long-term (2002–2014) evolution and trend in Collection 5.1 Level-2 aerosol products derived from the MODIS and MISR sensors over the Chinese Yangtze River Delta. *Atmos. Res.* **181**: 29–43. https://doi.org/10.1016/j.atmosres.2016.06.008.

Kaskaoutis DG, Kambezidis HD, Hatzianastassiou N, Kosmopoulos PG, Badarinath KVS. 2007. Aerosol climatology: dependence of the Angstrom exponent on wavelength over four AERONET sites. *Atmos. Chem. Phys. Discuss.* **7**: 7347–7397. https://doi.org/10.5194/acpd-7-7347-2007.

Kaskaoutis DG, Badarinath KVS, Kharol SK, Sharma AR, Kambezidis HD. 2009. Variations in the aerosol optical properties and types over the tropical urban site of Hyderabad, India. *J. Geophys. Res.* **114**: D22204. https://doi.org/10.1029/2009JD012423.

Kerandi NM, Laux P, Arnault J, Kunstmann H. 2017. Performance of the WRF model to simulate the seasonal and interannual variability of hydrometeorological variables in East Africa: a case study for the Tana River basin in Kenya. *Theor. Appl. Climatol.* **130**: 401–418. https://doi.org/10.1007/s00704-016-1890-y.

Kinney PL, Gatari GM, Volavka-close N, Ngo N, Ndiba PK, Law A, Gachanja A, Gaita MS, Chillrud NS, Sclar E. 2011. Traffic impacts on $PM_{2.5}$ air quality in Nairobi, Kenya. *Environ. Sci. Policy* **14**: 369–378. https://doi.org/10.1016/j.envsci.2011.02.005.

Kumar KR, Sivakumar V, Reddy RR, Gopal KR, Adesina AJ. 2013. Inferring wavelength dependence of AOD and Ångström exponent over a sub-tropical station in South Africa using AERONET data: influence of meteorology, long-range transport and curvature effect. *Sci. Total Environ.* **461–462**: 397–408.

Kumar KR, Sivakumar V, Yin Y, Reddy RR, Kang N, Diao Y, Adesina AJ, Yu X. 2014a. Long-term (2003–2013) climatological trends and variations in aerosol optical parameters retrieved from MODIS over three stations in South Africa. *Atmos. Environ.* **95**: 400–408. https://doi.org/10.1016/j.atmosenv.2014.07.001.

Kumar KR, Sivakumar V, Reddy RR, Gopal KR, Adesina AJ. 2014b. Identification and classification of different aerosol types over a sub-tropical rural site in Mpumalanga, South Africa: seasonal variations as retrieved from the AERONET sunphotometer. *Aerosol Air Qual. Res.* **14**: 108–123. https://doi.org/10.4209/aaqr.2013.03.0079.

Kumar KR, Yin Y, Sivakumar V, Kang N, Yu X, Diao Y, Adesina AJ, Reddy RR. 2015. Aerosol climatology and discrimination of aerosol types retrieved from MODIS, MISR and OMI over Durban (29.88°S, 31.02°E), South Africa. *Atmos. Environ.* **117**: 9–18. https://doi.org/10.1016/j.atmosenv.2015.06.058.

Kumar KR, Kang N, Sivakumar V, Griffith D. 2017. Temporal characteristics of columnar aerosol optical properties and radiative forcing (2011–2015) measured at AERONET's Pretoria_CSIR_DPSS site in South Africa. *Atmos. Environ.* **165**: 274–289.

Kumar KR, Kang N, Yin Y. 2018. Classification of key aerosol types and their frequency distributions based on satellite remote sensing data at an industrially polluted city in the Yangtze River Delta, China. *Int. J. Climatol.* **38**(1): 320–336. https://doi.org/10.1002/joc.5178.

Lau KM, Kim MK, Kim KM. 2006. Asian summer monsoon anomalies induced by aerosol direct forcing: the role of the Tibetan Plateau. *Clim. Dyn.* **26**: 855–864. https://doi.org/10.1007/s00382-006-0114-z.

Levy RC, Remer LA, Mattoo S, Vermote EF, Kaufman YJ. 2007. Second-generation operational algorithm: retrieval of aerosol properties over land from inversion of moderate resolution imaging spectroradiometer spectral reflectance. *J. Geophys. Res. Atmos.* **112**: 1–21. https://doi.org/10.1029/2006JD007811.

Levy RC, Remer LA, Kleidman RG, Mattoo S, Ichoku C, Kahn R, Eck TF. 2010. Global evaluation of the collection 5 MODIS dark-target aerosol products over land. *Atmos. Chem. Phys.* **10**: 10399–10420.

Liebmann B, Hoerling MP, Funk C, Bladé I, Dole RM, Allured D, Quan X, Pegion P, Eischeid JK. 2014. Understanding recent eastern horn of Africa rainfall variability and change. *J. Clim.* **27**: 8630–8645. https://doi.org/10.1175/JCLI-D-13-00714.1.

Liu Z, Liu Q, Lin HC, Schwartz CS, Lee YH, Wang T. 2011. Three-dimensional variational assimilation of MODIS aerosol optical depth: implementation and application to a dust storm over East Asia. *J. Geophys. Res. Atmos.* **116**: 1–19. https://doi.org/10.1029/2011jd016159.

Luo Y, Zheng X, Zhao T, Chen J. 2014. A climatology of aerosol optical depth over China from recent 10 years of MODIS remote sensing data. *Int. J. Climatol.* **34**: 863–870. https://doi.org/10.1002/joc.3728.

Mabasi T. 2009. Assessing the impacts, vulnerability, mitigation and adaptation to climate change in Kampala City. In *Fifth Urban Research Symposium*, 1–15. https://doi.org/10.1017/CBO9781107Q17415324.004 (accessed 14 October 2017).

Maidment RI, Allan RP, Black E. 2015. Recent observed and simulated changes in precipitation over Africa. *Geophys. Res. Lett.* **42**: 8155–8164. https://doi.org/10.1002/2015GL065765.

Makokha JW, Angeyo HK. 2013. Investigation of radiative characteristics of the Kenyan atmosphere due to aerosols using sun spectrophotometry measurements and the GOCART model. *Aerosol Air Qual. Res.* **13**: 201–208.

Makokha JW, Odhiambo JO, Godfrey JS. 2017. Trend analysis of aerosol optical depth and Ångström exponent anomaly over East Africa. *Atmos. Clim. Sci.* **7**: 588–603. https://doi.org/10.4236/acs.2017.74043.

Mehta M. 2015. A study of aerosol optical depth variations over the Indian region using thirteen years (2001–2013) of MODIS and MISR Level 3 data. *Atmos. Environ.* **109**: 161–170. https://doi.org/10.1016/j.atmosenv.2015.03.021.

Mehta M, Singh R, Singh A, Singh N, Anshumali. 2016. Recent global aerosol optical depth variations and trends – a comparative study using MODIS and MISR Level 3 datasets. *Remote Sens. Environ.* **181**: 137–150. https://doi.org/10.1016/j.rse.2016.04.004.

Mito CO, Boiyo RK, Laneve G. 2012. A simple algorithm to estimate sensible heat flux from remotely sensed MODIS data. *Int. J. Remote Sens.* **33**: 6109–6121. https://doi.org/10.1080/01431161.2012.680616.

Moorthy KK, Babu SS, Satheesh SK. 2005. Aerosol characteristics and radiative impacts over the Arabian Sea during the intermonsoon season: results from ARMEX field campaign. *J. Atmos. Sci.* **62**: 192–206. https://doi.org/10.1175/JAS-3378.1.

Ngaina JN, Muthama JM. 2014. Monitoring spatial-temporal variability of aerosol over Kenya. *Ethiop. J. Environ. Stud. Manage.* **7**: 244–252. https://doi.org/10.4314/ejesm.v7i3.2.

Ngo NS, Gatari M, Yan B, Chillrud SN, Bouhamam K, Kinney PL. 2015. Occupational exposure to roadway emissions and inside informal settlements in sub-Saharan Africa: a pilot study in Nairobi, Kenya. *Atmos. Environ.* **111**: 179–184. https://doi.org/10.1016/j.atmosenv.2015.04.008.

Ogwang BA, Chen H, Li X, Gao C. 2016. Evaluation of the capability of RegCM4.0 in simulating east African climate. *Theor. Appl. Climatol.* **124**: 303–313. https://doi.org/10.1007/s00704-015-1420-3.

Ongoma V, Chen H. 2017. Temporal and spatial variability of temperature and precipitation over East Africa from 1951 to 2010. *Meteorol. Atmos. Phys.* **129**: 131–144. https://doi.org/10.1007/s00703-016-0462-0.

Pace G, Sarra A, Meloni D, Piacentino S, Chamard P. 2006. Aerosol optical properties at Lampedusa (Central Mediterranean). Influence of transport and identification of different aerosol types. *Atmos. Chem. Phys. Discuss.* **5**: 4929–4969. https://doi.org/10.5194/acpd-5-4929-2005.

Panicker AS, Lee DI, Kumkar YV, Kim D, Maki M, Uyeda H. 2013. Decadal climatological trends of aerosol optical parameters over three different environments in South Korea. *Int. J. Climatol.* **33**: 1909–1916. https://doi.org/10.1002/joc.3557.

Prasad AK, Singh RP. 2007. Comparison of MISR-MODIS aerosol optical depth over the Indo-Gangetic Basin during the winter and summer seasons (2000–2005). *Remote Sens. Environ.* **107**: 109–119. https://doi.org/10.1016/j.rse.2006.09.026.

Ramanathan V, Feng Y. 2009. Air pollution, greenhouse gases and climate change: global and regional perspectives. *Atmos. Environ.* **43**: 37–50. https://doi.org/10.1016/j.atmosenv.2008.09.063.

Ramanathan V, Crutzen PJ, Kiehl JT, Rosenfeld D. 2001. Aerosols, climate, and the hydrological cycle. *Science* **294**: 2119–2124. https://doi.org/10.1126/science.1064034.

Remer LA, Kaufman YJ, Tanré D, Mattoo S, Chu DA, Martins JV, Li R-R, Ichoku C, Levy RC, Kleidman RG, Eck TF, Vermote E, Holben BN. 2005. The MODIS aerosol algorithm, products, and validation. *J. Atmos. Sci.* **62**: 947–973. https://doi.org/10.1175/JAS3385.1.

Robles-Gonzalez C, de Leeuw G. 2008. Aerosol properties over the SAFARI-2000 area retrieved from ATSR-2. *J. Geophys. Res.* **113**: D05206. https://doi.org/10.1029/2007JD008636.

Rosenfeld D. 2000. Suppression of rain and snow by urban and industrial air pollution. *Science* **287**: 1793–1796. https://doi.org/10.1126/science.287.5459.1793.

Sayer AM, Hsu NC, Bettenhausen C, Jeong M-J. 2013. Validation and uncertainty estimates for MODIS Collection 6 'Deep Blue' aerosol data. *J. Geophys. Res.* **118**: 7864–7872. https://doi.org/10.1002/jgrd.50600.

Sayer AM, Munchak LA, Hsu NC, Levy RC, Bettenhausen C, Jeong MJ. 2014. MODIS Collection 6 aerosol products: comparison between aqua's E-Deep Blue, Dark Target, and 'merged' data sets, and usage recommendations. *J. Geophys. Res. Atmos.* **119**: 13965–13989. https://doi.org/10.1002/2014JD022453.

Sayer AM, Hsu NC, Bettenhausen C, Jeong M, Meister G, Al SET. 2015. Effect of MODIS Terra radiometric calibration improvements on Collection 6 Deep Blue aerosol products: validation and Terra/Aqua consistency. *J. Geophys. Res. Atmos.* **120**(23): 12157–12174.

Tan C, Zhao T, Xu X, Liu J, Zhang L, Tang L. 2015a. Climatic analysis of satellite aerosol data on variations of submicron aerosols over East China. *Atmos. Environ.* **123**: 392–398. https://doi.org/10.1016/j.atmosenv.2015.03.054.

Tan F, Lim HS, Abdullah K, Yoon TL, Holben B. 2015b. Monsoonal variations in aerosol optical properties and estimation of aerosol optical depth using ground-based meteorological and air quality data in peninsular Malaysia. *Atmos. Chem. Phys.* **15**: 3755–3771. https://doi.org/10.5194/acp-15-3755-2015.

Tanré D, Kaufman YJ, Herman M, Mattoo S. 1997. Remote sensing of aerosol properties over oceans using the MODIS/EOS spectral radiances. *J. Geophys. Res.* **102**: 16971. https://doi.org/10.1029/96JD03437.

Torres O, Tanskanen A, Veihelmann B, Ahn C, Braak R, Bhartia PK, Veefkind P, Pieternel L. 2007. Aerosols and surface UV products form ozone monitoring instrument observations: an overview. *J. Geophys. Res. Atmos.* **112**: 1–14. https://doi.org/10.1029/2007jd008809.

Tripathi SN, Dey S, Chandel A, Srivastava S, Singh RP, Holben BN. 2005. Comparison of MODIS and AERONET derived aerosol optical depth over the Ganga Basin, India. *Ann. Geophys.* **23**: 1093–1101.

Twomey SA. 1977. The influence of pollution on the shortwave albedo of clouds. *J. Atmos. Sci.* **34**: 1149–1152.

Van Vliet EDS, Kinney PL. 2007. Impacts of roadway emissions on urban particulate matter concentrations in sub-Saharan Africa: new evidence from Nairobi, Kenya. *Environ. Res. Lett.* **2**: 1–5. https://doi.org/10.1088/1748-9326/2/4/045028.

Weatherhead EC, Reinsel GC, Tiao GC, Meng XL, Choi D, Cheang WK, Keller T, DeLuisi J, Wuebbles DJ, Kerr JB, Miller AJ, Oltmans SJ, Frederick JE. 1998. Factors affecting the detection of trends: statistical considerations and applications to environmental data. *J. Geophys. Res*. **103**: 17149–17161. https://doi.org/10.1029/98jd00995.

Welton EJ, Campbell JR. 2002. Micropulse lidar signals: uncertainty analysis. *J. Atmos. Oceanic Technol.* **19**: 2089–2094. https://doi.org/10.1175/1520-0426(2002)019<2089:MLSUA>2.0.

Yang W, Seager R, Cane MA, Lyon B. 2015. The annual cycle of East African precipitation. *J. Clim.* **28**: 2385–2404. https://doi.org/10.1175/jcli-d-14-00484.1.

Yu X, Kumar KR, Lü R, Ma J. 2016. Changes in column aerosol optical properties during extreme haze-fog episodes in January 2013 over urban Beijing. *Environ. Pollut.* **210**: 217–226. https://doi.org/10.1016/j.envpol.2015.12.021.

Zhang J, Reid JS. 2010. A decadal regional and global trend analysis of the aerosol optical depth using a data-assimilation grade over-water MODIS and Level 2 MISR aerosol products. *Atmos. Chem. Phys.* **10**: 10949–10963.

